Adaptive Image Inversion of Contrast 3D Echocardiography

By

Anjuman Shaheen
NUST201260801MSEECS61312F
MSCS-2
Department of Computing, SEECS, NUST

Supervised by
Dr. Kashif Mahmood Rajpoot
Assistant Professor
Department of Computing, SEECS, NUST

This thesis is submitted in partial fulfillment of the requirements for the degree of Masters of Science in Computer Science (MSCS)

School of Electrical Engineering and Computer Science (SEECS),
National University of Sciences and Technology (NUST), Islamabad, Pakistan

Date: January, 2015

Approval

It is certified that the contents of this thesis titled "**Adaptive Image Inversion of Contrast 3D Echocardiography**" submitted by **Anjuman Shaheen** have been found satisfactory for the requirement of the degree.

Advisor: Dr. Kashif Mahmood Rajpoot

Signature: _____

Date: _____

Committee Member 1: Dr. Sohail Iqbal

Signature: _____

Date: _____

Committee Member 2: Dr. Anis ur Rehman

Signature: _____

Date: _____

Committee Member 3: Dr. Omar Arif

Signature: _____

Date: _____

This thesis is dedicated to my respected father Mr. Noor Muhammad for his cooperation, encouragement and full support in my education career.

CERTIFICATE OF ORIGINALITY

I hereby declare that the thesis work titled "**Adaptive Image Inversion of Contrast 3D Echocardiography**" is my original work carried out as a post graduate student of computer science at the School of Electrical Engineering and Computer Science (SEECS), National University of Sciences and Technology (NUST). To the best of my knowledge, this thesis report has no materials previously published or written by another person, nor material which to a significant extent has been accepted for the award of any degree or diploma at NUST or any other education institute, except where due acknowledgment, is made in the thesis. Any contribution made to the research by others, with whom I have worked at NUST SEECS, or elsewhere, is explicitly acknowledged in the thesis.

I also declare that the intellectual content of this thesis is the product of my own work, except to the extent that assistance from others in the project's design and conception or in style, presentation and linguistic is acknowledged. All sources used for the research study has been fully and properly cited. I have also verified the originality of contents through plagiarism software.

Author Name: Anjuman Shaheen

Signature: _____

Date: _____

Acknowledgement

I am grateful to Allah Almighty who gave me courage and strength to complete this thesis work and all its requirements. I would like to express my thanks and regard to Dr. Kashif Mahmood Rajpoot (Assistant Professor of SEECS, NUST) for his kind attention, precious time and guidance during this thesis. The supervision and support that he gave truly helped the progression and smooth conduct of my work.

I want to thank my respected teachers who taught me throughout my MS course work and gave valuable information, suggestions and guidance in the compilation of my work. I specially thank my thesis committee members Dr. Sohail Iqbal, Dr. Anis ur Rehman and Dr. Omar Arif for their support, giving quality comments for work improvement and becoming a part of this work.

I am also thankful to SEECS management for providing excellent environment and facilities and all those who have helped me.

Last but not least, I pay my cordial thanks to my comrade Ruqayya Awan and my siblings for courageous support throughout my MS program and research thesis.

ABSTRACT

Contrast 3D echocardiography (C3DE) is commonly used to enhance the visual quality of ultrasound images in comparison with non-contrast 3D echocardiography (3DE). Though the image quality in C3DE is perceived to be improved for visual analysis, but it actually deteriorates for the purpose of automatic or semi-automatic analysis due to high speckle noise and intensity inhomogeneity. Therefore, the left ventricle (LV) endocardial feature extraction and segmentation from C3DE images remains a challenging problem. To overcome this challenge, this research work proposes a simple adaptive preprocessing method to invert the appearance of C3DE image. In this inverted appearance, the LV cavity appears dark while the myocardium appears bright making it similar looking to a 3DE image. Moreover, the resulting inverted image has high contrast and low noise appearance, yielding strong LV endocardium boundary and facilitating feature extraction for segmentation.

Our proposed image inversion mapping is based on an image intensity level threshold value, therefore our major contribution in this work is presenting an automatic threshold estimation (ATE) method through histogram analysis. This technique is validated through rigorous qualitative and quantitative measuring methods and favorable results are achieved. The results demonstrate that the inverse appearance of contrast image enables and simplifies the subsequent LV segmentation process. We highlight that the proposed method is the first attempt of its kind towards preprocessing technique and automatic/semi-automatic LV segmentation from C3DE images.

List of Contents

1. Chapter 1: Introduction 1

1.1 Motivation 4

1.2 Problem Statement 5

1.3 Approach 5

1.4 Thesis Contribution 5

1.5 Thesis Overview 6

2. Chapter 2: Background and Literature Review 7

2.1 Cardiac Imaging Modalities 8

2.1.1 Cardiac Ultrasound Images 8

Echocardiography 8

Contrast Echocardiography 11

2.1.2 Other Cardiac Imaging Modalities 12

Cardiovascular Magnetic Resonance Imaging (CMRI) 13

Computed Tomography (CT) 14

2.2 Image Preprocessing Methods 14

2.2.1 Image Intensity Transformation in Spatial Domain 15

2.2.2 Image Histogram 18

2.2.3 Related Work in C3DE Image Preprocessing 19

2.3 Left Ventricle Segmentation 20

2.4 C3DE Image Issues 22

2.5 C3DE Feature Extraction 23

2.6 Preprocessing Method Application on C3DE Images 25

2.6.1 Log Transformation 25

2.6.2 Power Law Transformation 25

2.7 Summary 26
3 Chapter 3: Proposed Methodology 28
3.1 Inverse Image Construction 29
3.2 Threshold Estimation 30
3.2.1 Data Analysis and Training 30
3.2.2 Automatic Threshold Estimation (ATE) 33
3.3 Summary 33
4. Chapter 4: Experiments and Results 34
4.1 Implementation 35
4.1.1 Experimental Data 35
4.1.2 Data analysis and training 35
4.1.3 Automatic Threshold Estimation 37
4.1.4 Inverse Image Construction 37
4.2 Validation Measures and Results 38
4.2.1 Validation of ATE 38
4.2.2 Validation by Semi-Automatic Segmentation 40
4.3 Discussion 42
4.3.1 Automatic Threshold Estimation (ATE) 42
4.3.2 Semi-Automatic Segmentation 43
4.4 Summary 46
5. Chapter 5: Conclusion and Future Work 47
5.1 Conclusion 48
5.2 Future Work 48
5.2.1 Validation on Larger Dataset 49
5.2.2 C3DE Image Homogenization 49

5.2.3 3DE Image Segmentation Methods and Commercial Tools 49

5.2.4 Comparison of C3DE Images with Non-Contrast 3DE 50

References 51

List of Figures

Figure 1.1: Echocardiographs, arrows indicating intensity drop out and missing anatomical structures. 3
Figure 1.2: Comparison of image appearance between echocardiography and contrast echocardiography 4
Figure 2.1: Two methods of acquiring echocardiography 9
Figure 2.2: Three views of 3DE. 10
Figure 2.3: Microbubbles in vitro with red blood cells (Courtesy Mallinckrodt Inc.) 11
Figure 2.4: Three views of C3DE. 12
Figure 2.5: Cardiac three views of CMRI imaging. 13
Figure 2.6: Cardiac three views of CT imaging. 14
Figure 2.7: Graph representation of intensity transformation functions. 16
Figure 2.8: Results of image negative transformation. 16
Figure 2.9: Logarithmic transformation function 17
Figure 2.10: Results of power law transformation function. 18
Figure 2.11: Examples of image enhancement by using histogram 19
Figure 2.12: Cardiac morphological structure 21
Figure 2.13: 2D slice selected from contrast 3D echocardiography. 23
Figure 2.14: Sobel edge detection of left ventricle in contrast echocardiograph. 23
Figure 2.15: Canny edge detection of left ventricle in contrast echocardiograph. 24
Figure 2.16: Log transformation of C3DE, (b) the results of log transformation with the constant value two and (c) the canny edge detection with the threshold value [0.01, 0.1]. 25
Figure 2.17 : Power law transformation of C3DE images. 26
Figure 3.1: C3DE inverse image construction. 29
Figure 3.2 : Three types of C3DE image gray level histogram shapes, ... 31
Figure 3.5: Inverted C3DE image using information from Histogram plot of C3DE image. 32
Figure 4.1: Results of C3DE image inversion by automatic threshold estimation 37
Figure 4.2: C3DE image inversion and non-contrast 3DE 40
Figure 4.3: C3DE segmentation process and the obtained result. (f) is an overlay of reference LV boundary (in red) and segmented LV boundary (in green) 44

Figure 4.4: C3DE segmentation process and the obtained result. (f) is an overlay of reference LV boundary (in red) and segmented LV boundary (in green). 45
Figure 5.1: 2D slice of contrast 3D echocardiography. 49

List of Tables

Table 4.1: Trained C3DE data of category 1 36
Table 4.2: Trained C3DE data of category 2 36
Table 4.3: Trained C3DE data of category 3 36
Table 4.4: Results of validation, training on ED images and validation on ED images,..... 39
Table 4.5: Results of validation, training on ES images and validation on ES images, ... 39
Table 4.6: Results of validation, training on ES images and validation on ED images, ... 39
Table 4.7: Results of validation, training on ED images and validation on ES images, ... 39
Table 4.8: Results of LOO validation, ... 40
Table 4.9: Results of Dice similarity index 42
Table 4.10: Results of mean contour distance 42

Abbreviations

2D	2 Dimensional
3D	3 Dimensional
3DE	3D Echocardiography
ATE	Automatic Threshold Estimation
Bp	Bin Percentage
C3DE	Contrast 3D Echocardiography
CMRI	Cardiovascular Magnetic Resonance Imaging
CT	Computed Tomography
CVD	Cardiovascular Disease
DSI	Dice Similarity Index
ECG	Electrocardiography
ED	End Diastolic
ES	End Systolic
FoV	Field of View
FR	Frequency Relationship
LOO	Leave One Out Validation
LV	Left Ventricle
MCD	Mean Contour Distance
PF	Peak Frequency
RT3DE	Real-time 3D Echocardiography
TEE or TOE	Transoesophageal Echocardiography
TTE	Transthoracic Echocardiography

Chapter 1: Introduction

Cardiovascular disease (CVD) is the leading cause of deaths worldwide, more than any other disease with 1.9 million casualties and has 47% contribution to all deaths in Europe during 2012 [1] . To reduce the number of CVD mortality rate, it is necessary to have an efficient diagnostic method for timely detection and monitoring of disease status. For this purpose, cardiac imaging is the leading choice of cardiologist for diagnosis of CVD and the study of cardiac structure as well as its function. Cardiac function is determined by visually or quantitatively assessing and analyzing the left ventricle (LV) volume, LV wall motion and myocardial thickening. Cardiac imaging is useful not only for visual assessment but also for automatic or semi-automatic analysis using image processing. In medical imaging, cardiac image analysis is an active area of research to study heart function. The LV is the largest and most crucial cavity of heart because it supplies oxygenated nutritious blood to the whole body. Therefore, researchers typically focus on the delineation and segmentation of LV endocardium or epicardium boundaries.

A number of cardiac imaging modalities are available for assessing the structure and function of the heart, in order to diagnose any CVD symptoms. These imaging modalities are non-invasive and capture images from outside of the body. These modalities include:

- Magnetic resonance imaging (MRI)
- Computed tomography (CT)
- Single photon emission computed tomography (SPECT)
- Positron emission tomography (PET)
- Echocardiography (includes contrast echocardiography)

These modalities produce different results according to their specific acquisition physics and vary in image acquisition cost and time, the imaged field of view (FoV), the image details and resolution, the harmful effect to the body, etc. These imaging modalities allow acquiring dynamic images of the heart with different perspective, thus providing information which can be used to assess aberrant structure and function for the diagnosis of CVDs. These assessments are very crucial for the further treatment decisions of disease. Among these modalities, echocardiography is generally accepted as a quick, non-invasive, cost effective and practical method for examining and exploring cardiac structure as well as its function at rest and during stress. It has been the most frequently used cardiac imaging modality for the past few decades because of following traits:

a) Fast real time acquisition

b) Cost effective
c) Portable scanner
d) Non-invasive characteristic with no known health risk to the patient

Real-time three-dimensional echocardiography (3DE) is a recent addition to the echocardiography imaging scene [2]. In previous literature, it has been stated that the 3DE provides better results in accuracy to calculate volumetric measurements than 2D echocardiography [3] . Despite the fact of being widely used in a large proportion of patients, sometimes 3D echocardiography fails to produce diagnostically useful images [4]. The image quality is known to be affected by ultrasound physics and influenced by factors such as fat, rib spacing, ultrasound reflection angle, and lung disease. These factors may hinder in the echo signal leading to limited field of view and weakening of the signal; therefore echocardiography suffers with intensity dropout, missing features and noise like speckle. These artifacts may further lead to inaccurate assessment of cardiac structure and anomalous interpretation. Figure 1.1 presents examples of 3DE images having intensity dropout, where the arrows point to missing anatomical structure.

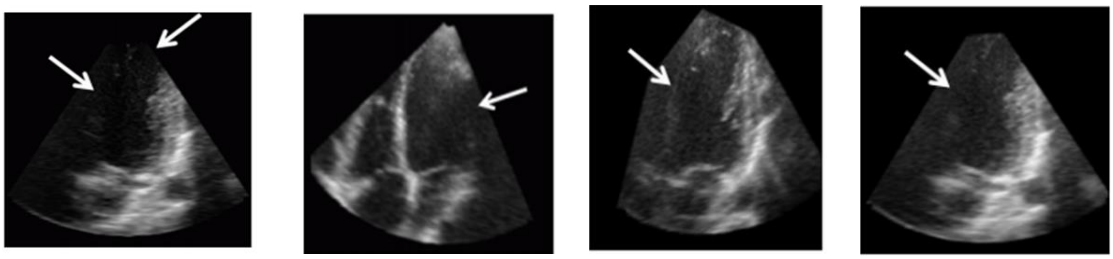

Figure 1.1: Echocardiographs, arrows indicating intensity drop out and missing anatomical structures [5].

To tackle these limitations, contrast enhanced echocardiography has emerged as an alternative choice to improve image quality for such cases, now with the introduction of contrast 3D echocardiography (C3DE). In contrast scans, drugs containing hyperechoic micro-bubbles are injected intravenously. These micro-bubbles are referred to as contrast agents. The ultrasound characteristic of these contrast agents is distinctly different from the blood and cardiac tissue. Contrast agents intravenously mixed in the blood produce strong backscatter in ultrasound waves, thus causing increase in the echocardiographic signal and resulting in better image quality [6].

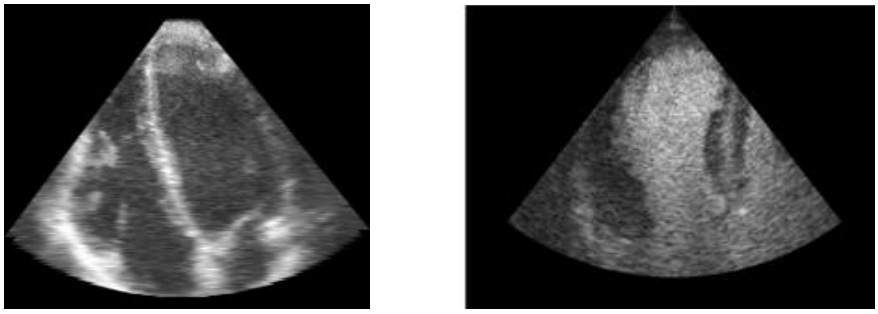

(a) Non-contrast echocardiograph (b) Contrast echocardiograph

Figure 1.2: Comparison of image appearance between echocardiography and contrast echocardiography [7].

Concentration of micro-bubbles in left ventricle (LV) blood pool is much higher than in vessels of cardiac muscles, thus resulting in inverted image appearance (see Figure 1.2) compared with routine echocardiography image and defines a clear LV endocardium boundary [7]. The visual appearance of endocardial delineation is often perceived to be improved in contrast echocardiography, thus enhancing the cardiologist's diagnostic ability with previously mentioned traits of 3DE. Cardiologists often prefer contrast images over non contrast images, in particular when corresponding non-contrast image quality is poor.

1.1 Motivation

Though the image quality in C3DE is perceived to be improved for visual analysis contrary to 3DE, but it actually deteriorates for the purpose of automatic or semi-automatic analysis due to high speckle and intensity inhomogeneity. The biggest hurdle in automatic or semi-automatic C3DE segmentation is the relatively low image contrast and intensity inhomogeneity inside blood pool left ventricle (LV) cavity (see Figure 1.2 (b)). In the C3DE images due to inverted appearance compared to 3DE, the LV segmentation methods proposed for 3DE images fail on the C3DE images. Moreover, the commercial softwares (QLAB and TomTec) do not presently support automatic or semi-automatic C3DE segmentation. Therefore, the left ventricle (LV) endocardial feature extraction and segmentation from C3DE images remain a challenging problem. In the previous literature, no considerable work has been done to address these issues. Therefore, there is a genuine need for the exploration of digital processing of C3DE to develop a preprocessing technique for C3DE image enhancement. This technique may assist in the subsequent visual assessment and towards automated analysis i.e. LV feature extraction and segmentation.

1.2 Problem Statement

This work proposes an adaptive automatic preprocessing technique in which the new inverted representation of a C3DE image is constructed to overcome image inhomogeneity and speckle noise. This inverted representation facilitates the further automatic/semi-automatic analysis.

1.3 Approach

In this work, we propose a simple approach to confront the C3DE image poor quality by developing an image pre-processing technique. In this adaptive technique, the inverse representation of a C3DE image is constructed by finding a threshold based on the image histogram properties. In this inverted appearance, the LV cavity appears dark while the myocardium appears bright similar to a 3DE image. Moreover, the resulting inverted image has high contrast and low noise appearance, yielding strong LV endocardium boundary and facilitating feature extraction for segmentation.

1.4 Thesis Contribution

In this research work, we explore the C3DE to develop an adaptive pre-processing technique to deal with difficult and challenging C3DE images. This thesis makes following contributions:

- An adaptive pre-processing technique of inverse image construction is developed, to assist the subsequent C3DE image analysis i.e. left ventricle (LV) feature extraction and segmentation.
- Presented a novel method of automatic threshold estimation for the C3DE image inversion.
- Rigorously validated the proposed technique and achieved favorable results.
- This work is the first attempt of its kind towards preprocessing and automatic/semi-automatic LV segmentation form.

Moreover, a part of this thesis work has been accepted in the following conference:
"12th International Conference on Frontier of Information Technology, Islamabad, Pakistan", entitled with "An Adaptive Inverse Image Construction Method for Contrast 3D Echocardiography".

1.5 Thesis Overview

This thesis is structured as following.

Chapter 2 presents the relevant background to describe the important fundamental concepts about our work. It includes the cardiac imaging modalities with brief description of echocardiography, contrast echocardiography and some other modalities. Further, relevant literature on echocardiography image pre-processing techniques and LV segmentation is discussed. Further this chapter presents two main issues regarding C3DE images, which hinder the LV feature extraction and then subsequent segmentation. After that, intensity transformation preprocessing methods are applied and results are analyzed by the LV feature extraction.

Chapter 3 presents our methodology of C3DE image inversion in detail.

Chapter 4 discusses the validation of presented technique and their acquired results. It includes the different validation measures for automatic threshold estimation with results and discussions. Further this chapter presents semi-automatic segmentation and its results.

Chapter 5 presents the conclusion of the thesis work and future work.

Chapter 2: Background and Literature Review

This chapter provides the relevant background about this thesis. Cardiac imaging modalities are explored with their respective benefits and limitations. Moreover, relevant work is reviewed in this chapter.

2.1 Cardiac Imaging Modalities

The CVD suspected patient has to go through a series of diagnostic assessments, which includes patient and his kinship clinical study, physical examination, blood test and an electrocardiography (ECG) test. If these assessments provide the evidence of any CVD then other cardiac imaging based tests are recommended to detect the exact problem, so that the proper treatment against the detected CVD may be started. Thus, cardiac imaging based techniques are used in analysis and assessment of cardiac structure, cardiac morphology, hemodynamic and cardiac motion. In cardiac imaging, many imaging modalities have been used during last few decades. It is preferred to adopt a technique, which has less or no harmful effects to a patient to ensure the safety of patient's condition. The various cardiac imaging modalities are briefly described below.

2.1.1 Cardiac Ultrasound Images

Ultrasound imaging technique uses ultrasound waves, which have high frequency than the sound waves. The audible sound frequency range is 20 Hertz (Hz) to 20 KHz, and in cardiac image application ultrasound waves with the range of 1-20 MHz (million Hz) have been used [8]. In ultrasound imaging, a device called transducer is used for both generation and reception of ultrasound waves. In the ultrasound image acquisition, waves are emitted and their reflections and scatterings from an interface (i.e. body organ, soft tissue and blood of the heart) are recorded. These recordings are used in an image construction.

Hence, for the cardiac ultrasound imaging, echocardiography and contrast echocardiography are the first choice by the cardiologist with no known harmful side effects. Echocardiography and contrast echocardiography are briefly explained below.

Echocardiography

In early 1950's Hertz and Edler introduced echocardiography for dynamic cardiac imaging [9] and now it is widely used in the diagnosis, management, and follow-up of patients with any suspected or known CVD. Echocardiography uses the ultrasound waves with high frequency (3 – 5 MHz) to produce images of cardiovascular structure and captures the information of cardiac

structure, blood flow and the cardiac function. In echocardiography, transducer emits ultrasound waves which are then captured after their reflection from the tissue interfaces for image construction. This echo depends on the various factors like tissue's density, wave frequency and tissue's reflectance property. As reflectivity property of heart's tissues and components (blood, veins, and muscle fibers) is different, so they produce different intensity of echo yielding image construction.

In order to acquire echocardiography scans, there are two alternative techniques:

1) Transthoracic echocardiography (TTE): the transducer is placed over the chest or thorax area to acquire image scans, TTE is shown in Figure 2.1 (a).
2) Transoesophageal echocardiography (TEE or TOE): the probe device is passed through the oesophagus to acquire image scans TEE is shown in Figure 2.1 (b)

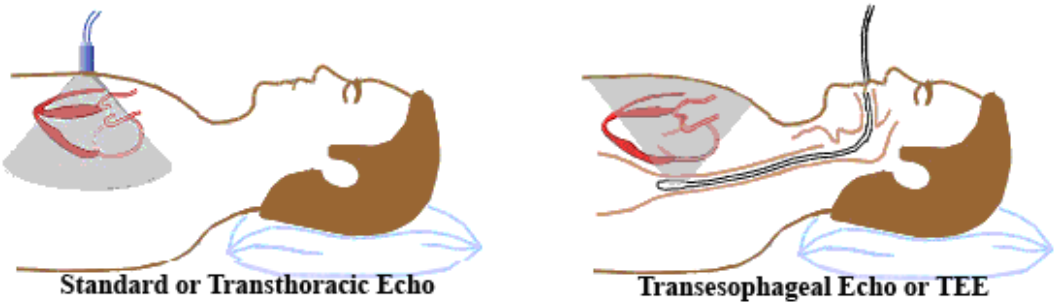

(a) Transthoracic echocardiography (TTE) (b) Transoesophageal echocardiography (TEE or TOE)

Figure 2.1: Two methods of acquiring echocardiography [10].

Among these two techniques, TEE provides better quality visualizations of cardiac structures than TTE because of the location of ultrasound probe close to heart. Despite of TEE giving better quality, TTE is more commonly used as it its fully non-invasive nature, thus friendly to a patient.

Initially, transducers were able to capture 1D + time image, which presented the movement and the thickness of cardiac components like cardiac wall, valves and blood flow. This limited 1D + time view was used for the further cardiac analysis but gradual advancement in transducer technology lead to better quality as well as dynamic range in imaging.

The 2D echocardiography allows visualizing and calculating more accurate measurements of the cardiac structure and function and the shape of the heart compared to 1D echocardiography. In 2D echocardiography, single or multiple image 2D scans are acquired from cardiac long axis or

short axis, but it has limitations to understand the complex 3D cardiac structure. Over the years, the researchers developed techniques to generate 3D scans of echocardiography with the advancement of transducer technology.

The 3D echocardiography (3DE) scans capture entire 3D cardiac volume and display in three views namely: (1) apical 2- chamber, (2) apical 4-chamber, and (3) short axis. It provides broad view of the heart, which improves the visualization of structure and function of the heart. The 3DE allows to capture and study the 3D morphology and dynamics of heart, at a low-cost and without associating any harmful effects. Figure 2.2 shows the three orthogonal views of an echocardiographic image.

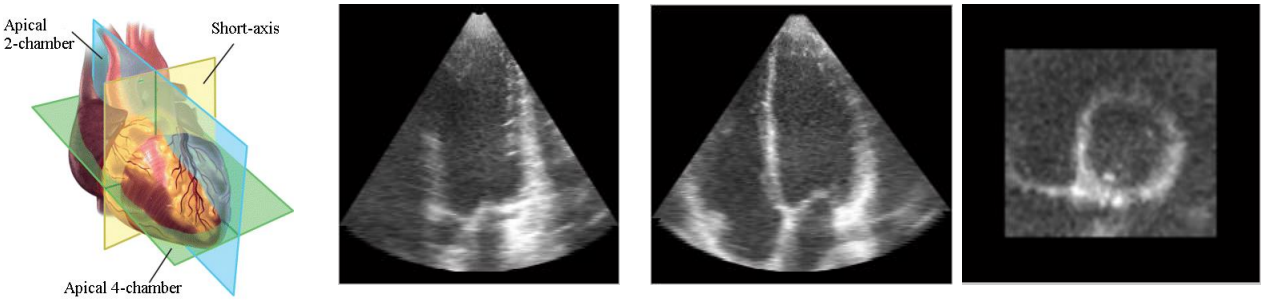

(a) A 3D cardiac model [11] (b) Apical 2- chamber view (c) Apical 4- chamber view (d) Short axis view

Figure 2.2: Three views of 3DE.

A 3D echocardiography image is constructed by two methods:

1) Reconstructed 3D echocardiograph: referring a method in which, multiple 2D plane images are taken via free hand movement or fixed mechanical movement of the conventional transducer [12], and then these images are geometrically processed to reconstruct a 3D image.
2) Volumetric 3D echocardiography: refers to the method in which an advanced transducer is used to acquire full 3D volume of a heart termed as real-time 3D echocardiography (RT3DE). In volumetric 3D echocardiography, a matrix array transducer is used to scan the image. In this thesis, volumetric 3D scans are used.

Nowadays, standard clinical hardware is available for 4D echocardiography (3D+time) acquisition that provides more clarification for the assessments of LV functions. Thus, it provides opportunities to analyze the dysfunction or anomalous cardiac structure.

Contrast Echocardiography

Echocardiography is widely used in cardiac imaging however in some patients it fails to produce good results (shown in Figure 1.1). The image quality is known to be affected by ultrasound physics and influenced by factors such as fat, rib spacing, ultrasound reflection angle, and lung disease which may lead to inaccurate assessment of cardiac structure and anomalous interpretation [4]. European Association of Echocardiography study [4] reveals that the echocardiographic images are suboptimal in as many as 33% of the patients [13]. Therefore, contrast echocardiography has emerged as an alternative to improve image quality for such cases. Contrast echocardiography utilizes the contrast agents, which are injected intravenously, to enhance the visualization and quality of images. For these patients, the visual appearance of endocardial delineation is often perceived to be improved in contrast echocardiography (see Figure 2.4), thus often enhancing the cardiologist's diagnosis ability.

In 1968, Gramiak and Shah [14] first used the gas bubbles in echocardiography for contrast images and then this technology was universally adopted for usage of free gas bubble to enhance the visualization in the echocardiography. Contrast agents consist of micro-bubbles of encapsulated high molecular weight filled with some gas (e.g., nitrogen) and strengthened by permeable shell consisting palmitic acid. They are injected into a patient bodyand are less toxic to avoid any side effects, small size of 1 – 4 micrometer in diameter, though they can freely move in blood circulatory system (capillaries, arterioles and venules) and have enough life stability for the duration of taking ultrasound scans [6]. The ultrasound characteristics of these micro-bubbles is distinctly different from the blood and cardiac tissue, as the backscattering property of blood and cardiac tissue is very less than these micro-bubbles, thus micro-bubbles respond strongly to the ultrasound waves and produce strong backscatter, causing increase in the echocardiographic signal and resulting in better image quality [4].

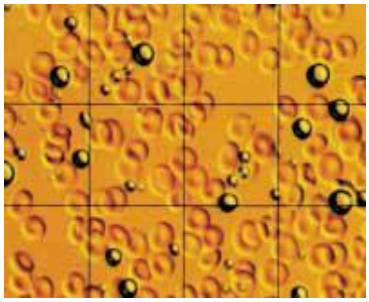

Figure 2.3: Microbubbles in vitro with red blood cells (Courtesy Mallinckrodt Inc.) [6].

Though, blood saturated with micro-bubbles passes (Figure 2.3) through the LV and vessels of the heart yield contrast enhanced image, and in left ventricle (LV) blood pool is much higher than in vessels of cardiac muscles, thus LV cavity appears brighter and myocardium appears darker contrary to non-contrast echocardiography. From contrast images (Figure 2.4), it can be clearly seen that LV cavity has high (bright) intensity due to presence of concentrated contrast agents in blood, and myocardium appear dark with low intensity values because of myocardium vessels containing less amount of blood than LV cavity. It is notable that contrast echocardiography improves the visual quality of image during rest and stress echocardiography (the echocardiographic scans are captured by putting the heart under some kind of physical or pharmacological stress). Often by using contrast echocardiographic scans, the more costly and more hazardous tests can be minimized, and fast diagnosis can be achieved.

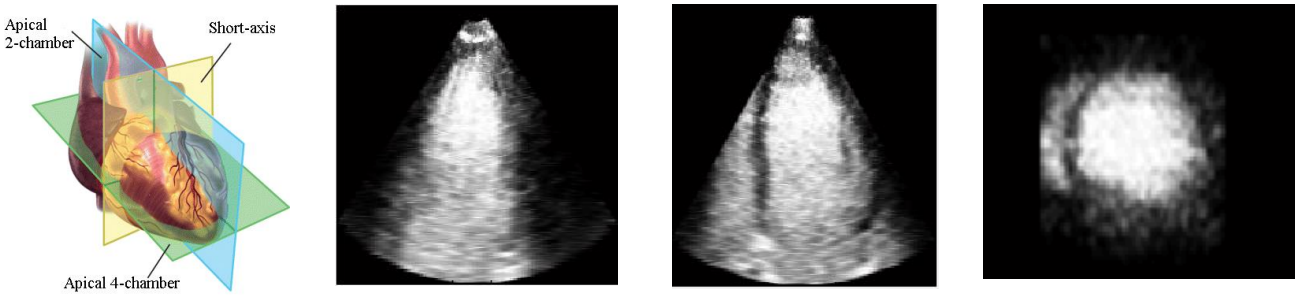

(a) A 3D cardiac model [11] (b) Apical 2- chamber view (c) Apical 4- chamber view (d) Short axis view

Figure 2.4: Three views of C3DE.

Cardiologists often prefer contrast images over non contrast images, in particular when non-contrast image quality is poor. In practice, contrast echocardiography is considered only as a replacement for conventional echocardiography because of intravenous injection and potential side-effects of the microbubbles to the body.

2.1.2 Other Cardiac Imaging Modalities

As described earlier, ultrasound imaging (echocardiography and contrast echocardiography) is the most widely used cardiac imaging modality; however it also has some inherent limitations regarding the image quality. The main limitation is the low resolution image than other imaging modalities (for example, MRI and CT), which results in missing or spurious cardiac features [15]. Speckle, limited field of view and attenuation in the image are other major limitations, which hinder the cardiac assessment. Thus, other cardiac modalities are also used for imaging;

these modalities may have good imaging quality but can by highly expensive in cost, hostile to a patient or may have harmful side effects to a patient. Some of these modalities are CT, MRI, PET, and SPECT.

Cardiovascular Magnetic Resonance Imaging (CMRI)

Cardiovascular magnetic resonance imaging, also known as cardiac MRI, is a non-invasive medical imaging modality for the cardiovascular system's structure and function assessment. It utilizes the basic principle of magnetic resonance imaging (MRI), with additional optimization by the use of electrocardiograph (ECG). The principle of magnetic resonance imaging (MRI) [16, 17] is based on the fact that the human body tissues contain water molecules with the hydrogen charged nuclei (proton and neutron) and each hydrogen nuclei has a magnetic spin property in arbitrary directions. When magnetic fields are applied to the human body, these nuclei absorb the radiation and get parallel alignment (nuclei having lower energy states) or anti-parallel alignment (nuclei having higher energy states) to this magnetic field. After that radiofrequency (RF) is applied, under weaker field of RF, nuclei return to their original state by emitting back the energy difference. This energy difference is measured for the image construction (shown in Figure 2.5) and yields fine image quality and resolution. Contrast enhanced CMRI is also used for cardiac assessment.

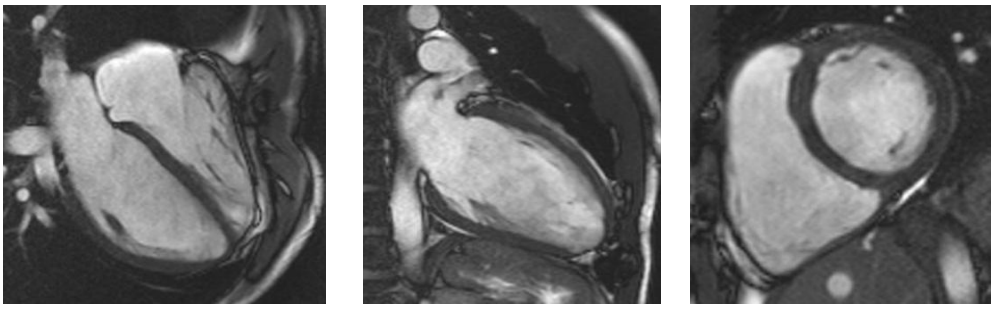

(a) 4 – chamber view (b) 2 – chamber view (c) Short axis

Figure 2.5: Cardiac three views of CMRI imaging [15].

In CMRI, because of unfriendly way of acquisition, the patients with claustrophobia may have problem during examination. However, the image quality of short axis view is adequate but the resolution of two chamber and four chamber views is typically very poor. Due to the usage of magnetic field, this modality is prohibited for those who have metallic cardiac pace makers or

metal implants. With respect to cost and portability, it is very expensive (in time and money) than conventional and contrast echocardiography.

Computed Tomography (CT)

In computed tomography, X-rays are used for image acquisition. The human body is exposed to X-rays by a circular tube known as gantry and then detected by the detector on same device for the image construction. CT cardiac views are shown in Figure 2.6 as an example. CT is highly dependent on the stillness of the body where slight movement can result in poor image quality. The benefits of cardiac CT are that it provides high spatial resolution and high temporal resolution and good quality visualization of arteries, but these radiations are appalling for the patient. Thus, cardiologists prefer CT for the cardiac blood vessels examination rather than cardiac volume and structure.

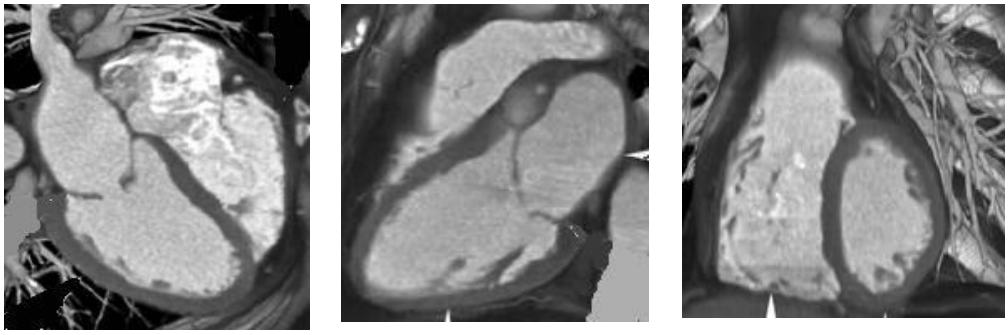

(a) 4 – chambered view (b) 2 – chambered view (c) short axis

Figure 2.6: Cardiac three views of CT imaging [15].

In summary, echocardiography is most commonly used cardiac imaging modality in every perspective i.e. have no side effects, low cost, portable and patient friendly, thus worldwide cardiologists practice this as their foremost choice for cardiac imaging and contrast echocardiography is preferred when non contrast results are poor.

Cardiac images are digitally processed in order to get semi-automatic or automatic analysis, thus image processing provides methods for noise reduction, feature extraction and identification etc.

2.2 Image Preprocessing Methods

The objective of image preprocessing is to manipulate and enhance an image in such a way that the resultant image becomes more suitable for desired further processing than original image for a specific application [18]. There are set of techniques which modify images to improve their interpretability for the visual and automatic or semi-automatic analysis [19]. Researchers are

paying intense attention on the development of image preprocessing techniques in order to assist subsequent further image analysis in different image processing fields i.e. medical imaging, geographical imaging, surveillance application etc.

As described above, in this thesis, we have developed a preprocessing technique of image inversion for C3DE image, this technique is based on spatial domain (intensity transformation).

In the following section, relevant preprocessing techniques in spatial domain are elaborated.

2.2.1 Image Intensity Transformation in Spatial Domain

Spatial domain is an image plane itself and methods in this category are based on direct manipulation of pixels in an image. The spatial domain intensity transformation of an image is denoted by the expression [18]:

$$g(x,y) = T[f(x,y)] \tag{2.1}$$

where $f(x,y)$ is the input image, $g(x,y)$ is the output image (processed), and T is a transformation operator on f defined over a point *(x, y)* [18].

Intensity transformation function (*T*) deals with a single point (1x1 pixel neighborhood) intensity transformation function is written in simplified form as,

$$S = T(r) \tag{2.2}$$

where r is input gray level value and S is the output transformed image $g(x,y)$ image. Figure 2.7 shows the representation of basic three intensity transform functions i.e. linear (negative and identity), logarithmic (log and inverse-log), and power-law (nth power and nth root) [18].

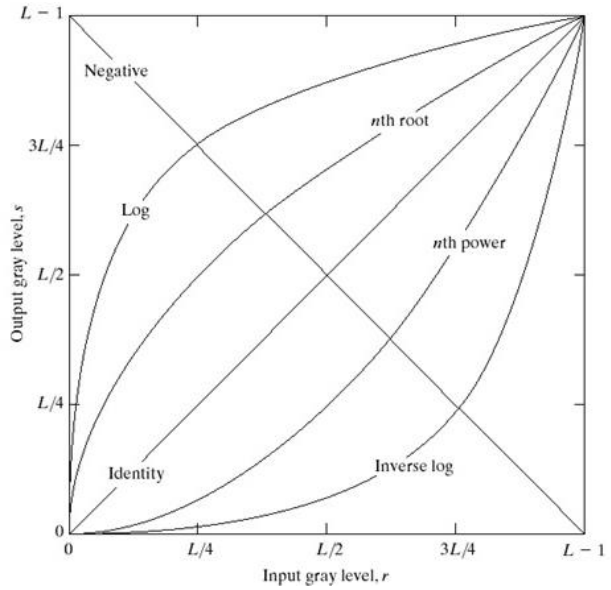

Figure 2.7: Graph representation of intensity transformation functions.

Linear (negative and identity), logarithmic (log and inverse-log), power-law (nth power and nth root) [18] transformations.

- Linear transformation function*:* It consists of identity transformation and negative transformation (see Figure 2.8). The identity function is a trivial case in which the image output image intensities are equal to input image intensities, while in negative transformation image intensities are transformed by the following function:

$$T(r) = L - 1 - r \tag{2.3}$$

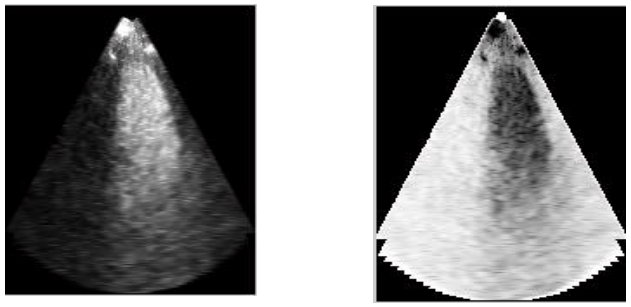

(a) Original Image (b) Image negative

Figure 2.8: Results of image negative transformation.

Negative transformation is useful in those cases, where it is needed to enhance white and gray details embedded in the dark region.

- Logarithmic transformation function: This transformation is carried out by using logarithm function:

$$S = clog(1 + r) \tag{2.4}$$

where *c* is constant and *r* is intensity value of input image. This transformation maps a narrow range of low intensity values of input into the wider range of output levels (Figure 2.9 is demonstrating this transformation).

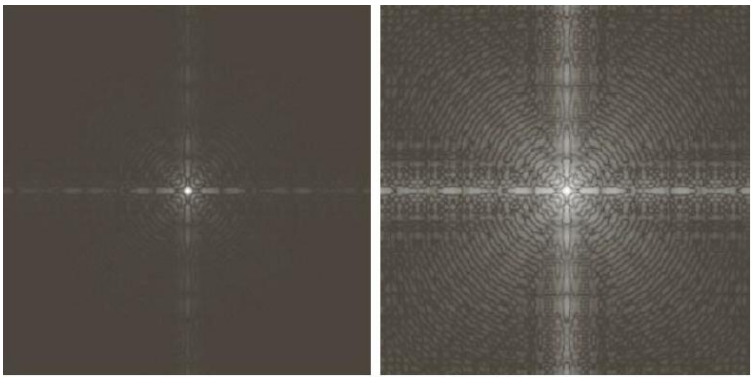

(a) Fourier transform (b) Result of equation (2.4)

Figure 2.9: Logarithmic transformation function [18].

- Power-law transformation function: This function is represented as:

$$S = cr^{\gamma} \tag{2.5}$$

where c and γ are the positive constants. The power law curve is shown in Figure 2.7. In this transformation fractional γ values (less than one) map a narrow range of input (dark) into a wider range output (bright), while γ values greater than one give the opposite effect. The Figure 2.10 shows the results of power law transformation.

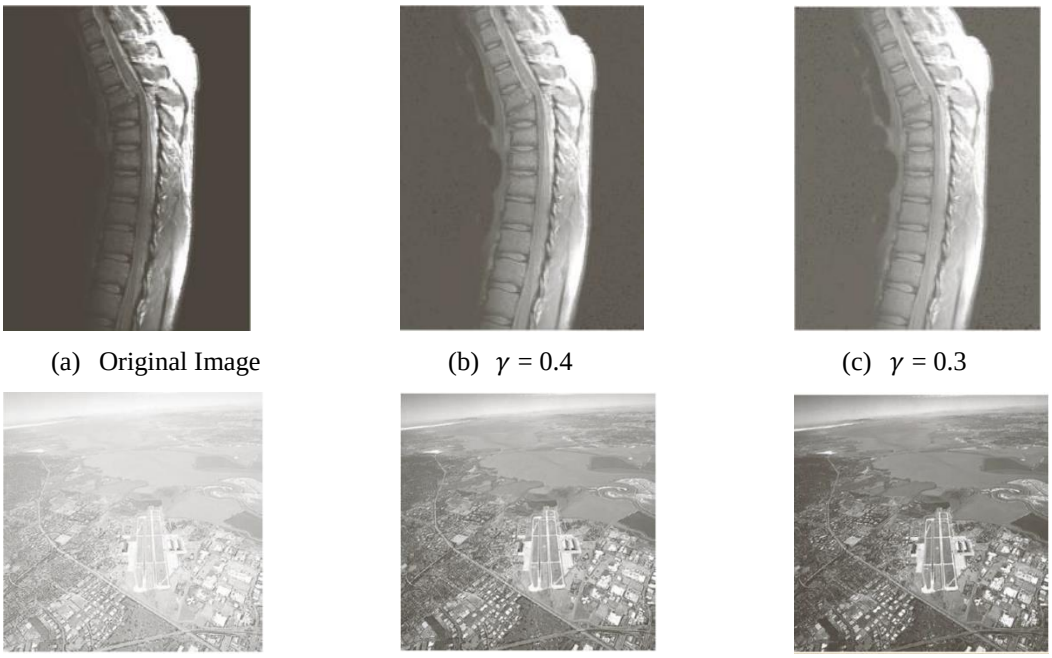

(a) Original Image (b) γ = 0.4 (c) γ = 0.3

(d) Original Image (e) γ = 3.0 (f) γ = 5.0

Figure 2.10: Results of power law transformation function.

Images (a) and (d) are original images, (b) and (c) are the results of power law transformation, where $\boldsymbol{\gamma}$ value is less than 1, (e) and (f) are the results of power law transformation, where $\boldsymbol{\gamma}$ value is greater than 1 [18].

2.2.2 Image Histogram

It plays an important role in image enhancement, pre-processing, compression, segmentation, and description. Histogram is the representation of frequency distribution of image pixel values. It represents the frequency (occurrence) of each intensity level in the entire image. The histogram of a digital image with *L* total possible intensity levels in the range [0, L-1] is defined as the discrete function:

$$h(r_k) = n_k \tag{2.6}$$

where r_k is the *kth* intensity level in the interval [0, L-1] and n_k is the number of pixels in the image whose intensity level is r_k.

Histogram processing is a powerful tool for image modifications. Some other histogram processing includes piecewise linear functions (contrast stretching and thresholding), which are

used in intensity transformation for getting desired results. Contrast stretching is a transformation that expands the intensity level range of an image such that it spans the full intensity range of output, while thresholding is to choose particular intensity value which separates the interested region (i.e. segmentation).

(a) Original image (b) Contrast stretching (c) Thresholding

Figure 2.11: Examples of image enhancement by using histogram [18].

In Figure 2.11, a low contrast 8 –bit image is given, which is being processed by contrast stretching (Figure 2.11 (b)) and thresholding (Figure 2.11 (c)). Histogram processing often assists in automatic processing and opens research areas to study more area specific to image enhancement techniques.

2.2.3 Related Work in C3DE Image Preprocessing

To the best of our knowledge, there has been no previous work in C3DE preprocessing method to assist subsequent image analysis. However, considerable work has been done in ultrasound and echocardiography image enhancement. Zwim and Akselrod [20] worked on a histogram based technique for the noise reduction in the echocardiographic images. Their technique is an adaptive method of brighter transfer function (BTF) which determines each specific echocardiographic cine loop's gray level characteristics. In this technique, automatic segmentation is performed based on the histogram, by using sum of three Gaussian functions for fitting which are correlated to different tissue types. This enhancement technique is tested on 23 cine-loops from ten different patients, and obtained results are clearly better in contrast and have richer gray-levels within the cardiac muscle. Tay et al. [21] presented a technique of speckle reduction and homogenization in cardiac ultrasound images. In their method, image homogenization is achieved by decreasing the pixel variation in the inhomogeneous region by an iterative method that at each iteration smoothes only outlying pixel values by local mean. Cheng and Tang [22] focused on speckle denoising technique in wavelet domain for the medical

ultrasounds images. The proposed technique consisted of the manipulation of wavelet coefficients by fusing the wavelet transform with robust support vector regression (SVR) estimation for the speckle noise reduction in ultrasound images. Chang et al. [23] presented an image contrast enhancement technique which is based on a histogram transformation of local standard deviation. Previous conventional image enhancement techniques entail noise over enhancement and ringing artifacts, so their adaptive contrast enhancement (ACE) algorithm has a capability to reduce noise and ringing effect while resulting in image enhancement. In the algorithm, contrast gains (CG) are used to adjust high frequency components in image. Initially authors build a mathematical model for the local standard deviation (LSD) distribution by extending Hunt's image model [24]. The local standard deviation CG is formulated as a non-linear function based on the transformation between the LSD histogram and a desired LSD distribution. It was noticed that conventional techniques formulate CG by linear function but in this approach the non-linear function are used to compute the CG's of an image which produces better results with little noise and ringing effect. Modersitzki and Wirtz [25] worked on combining homogenization and registration of general medical image data as well as real life image data. Their technique is based on the comparison of the reference image with template image. For the image homogenization, authors are using a threshold method for the comparison with reference image.

2.3 Left Ventricle Segmentation

In human heart, the major role of the cardiac ventricles is to pump blood, right ventricle pumps blood to the lungs and left ventricle pumps blood to the whole body. A decline in ventricular performance can lead to a substantial impact on heart function. Among four cardiac chambers, LV is the large cavity with thicker myocardium muscles which enable it to pump the oxygenated blood to the entire body; the cardiac structure is shown in Figure 2.12. From the past research [26], it has been shown that major CVDs are caused by LV dysfunctions. The major CVDs caused by LV dysfunction are: LV hypertrophy, myocardial ischemia and cardiomyopathy [27]. Therefore, cardiologists are particularly interested in detecting LV dysfunction, focusing especially on endocardium border to analyze its size and structure for the assessment of suspected CVD.

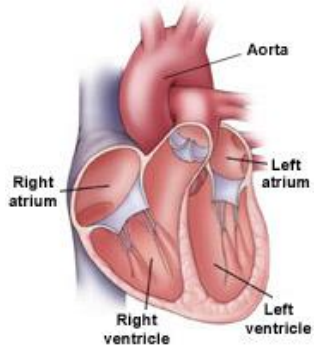

Figure 2.12: Cardiac morphological structure [28].

In ultrasound images, LV segmentation is a difficult problem due to signal attenuation, shadowing, intensity dropout, limited field of view, contrast inhomogeneity, and missing anatomical boundaries. Thus LV segmentation in this modality is a challenging and an active area of research. However, to the best of our knowledge, there has been only one previous work on LV segmentation from C3DE. Ma et al. [5] proposed an LV segmentation algorithm using 3D active shape models. The C3DE scans were obtained from a fast rotating ultrasound transducer (FRU) [5]. However, the FRU transducer is not commonly used in cardiology clinics due to the recent availability of volumetric matrix-array transducers by leading scanner manufacturers for C3DE scan acquisition. To the best of our knowledge, there has been no previous attempt in the published literature for LV segmentation from C3DE scans obtained from volumetric matrix-array transducer. This illustrates the challenge faced for LV segmentation from C3DE images.

Apart from contrast echocardiography, considerable research has been done recently on 3DE LV segmentation. A common approach has been to treat echocardiographic LV segmentation as a contour finding approach. Mignotte and Meunier [29] also used active contour model for the LV short axis segmentation, they used a statistical external energy in a discrete active contour for the segmentation, and according to their work it has been suggested that their method was suitable in ultrasound images to deal with significant noise and missing boundaries. Fully automated registration based LV segmentation is presented by Zagrodsky et al. [30]. For the speckle noise reduction, they applied median-filtering as pre-processing step. The registration assists by initializing the segmentation surface close to the endocardial border. The initialized surface was then deformed with a conventional snake attracted by a gradient vector flow field [31] constructed using a Sobel-edge operator. Rajpoot et al. [5] have conducted recent work in feature extraction using phase base method on the fused multi-view 3DE images and then LV

segmentation by active contour model. Angelini et al. [32] performed LV segmentation of real time 3D echocardiography. For the speckle reduction, the images are preprocessed by a wavelet analysis, and then a 2D deformable balloon model with an intensity gradient based force is used for the segmentation of individual slices. The method was tested on six clinical datasets while comparison was made with MR manual segmentation on ED and ES frames. Deopujari and Dubey [33] presented LV segmentation method using active contour model and low pass Gaussian smoothing is used for denoising.

2.4 C3DE Image Issues

In the conventional echocardiography, LV cavity appears black than the myocardium tissue (see, Figure 2.2) because the reflective property of blood is much weaker than the solid tissue. Thus the ultrasound waves scattered by red blood cells are very weak, which results in darker display of LV cavity region in the image [6]. Contrary to conventional echocardiography, in contrast scans, blood saturated with contrast agents yields LV blood pool in much brighter appearance than in vessels of cardiac muscles (Figure 2.4) which apparently improves the visual quality of image.

As described in previous section, despite of having advantage over non-contrast 3DE, the maximum utilization of C3DE images has been hampered due to difficult quality of image. C3DE image analysis faces the following issues which hinder the subsequent automatic or semi-automatic image analysis:

a) The ultrasound beam is reflected and scattered by many uncorrelated free moving contrast microbubbles within the LV cavity, so the image contains inhomogeneous texture characteristics. Contrast inhomogeneity refers to having varying intensity levels in the same region (see Figure 2.13 (a)). It can be seen that the encircled LV cavity has highly contrast inhomogeneity which hampers the subsequent visual assessment and segmentation of cardiac structure.

b) There is a relatively low contrast or slow intensity change between brighter LV cavity and myocardium border (see Figure 2.13 (b)). Moreover, in LV segmentation, endocardium LV feature extraction is considered an important pre-processing step before applying subsequent processes but in C3DE low contrast between myocardium border and LV cavity obstructs the traditional LV edge driven feature extraction.

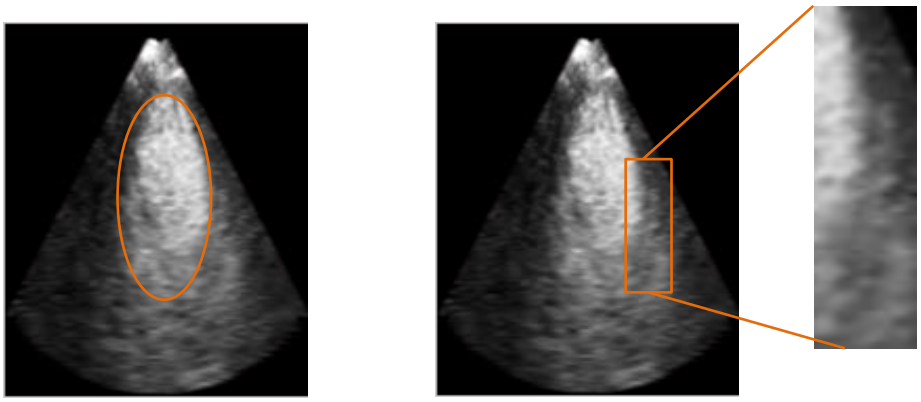

(a) Encircled LV cavity with contrast inhomogeneity (b) Myocardium border

Figure 2.13: 2D slice selected from contrast 3D echocardiography.

2.5 C3DE Feature Extraction

Feature extraction is required as a pre-processing step to facilitate subsequent LV segmentation. For such purpose edge detectors are used because edges define a change in an image and may refer to important information or feature i.e. LV cavity in C3DE images. However, in C3DE images, edge detection methods face not clearly defined edges due to issues mentioned earlier.

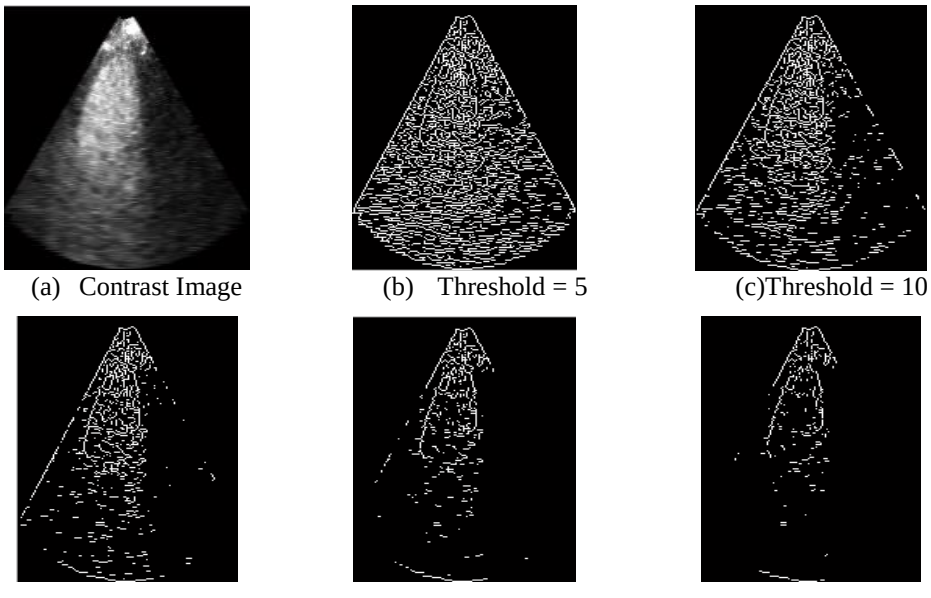

(a) Contrast Image (b) Threshold = 5 (c)Threshold = 10

(d) Threshold = 15 (e)Threshold = 20 (f) Threshold = 25

Figure 2.14: Sobel edge detection of left ventricle in contrast echocardiograph.

We have applied commonly used gradient intensity based edge detectors (Sobel, Canny) on the contrast images and results are shown in Figure 2.14 and Figure 2.15, but results are not satisfactory with respect to LV extraction.

In Sobel edge detection (Figure 2.14), edges are not clear to extract cardiac LV, while the variation in the threshold also does not provide the required results. Moreover, Figure 2.15 shows that Canny edge detection results are apparently better than Sobel but still not leading to proper extraction of LV endocardial features. The results from Figure 2.15 show that applying the threshold (low thresh = 0.01, high thresh = 0.1) on the contrast image provides relevant edges of LV but with also some additional spurious edges. It can be observed that by increasing the sigma of Gaussian smoothing (Figure 2.15, (d) to (f)), false edges are reduced but it also fades out the LV edges.

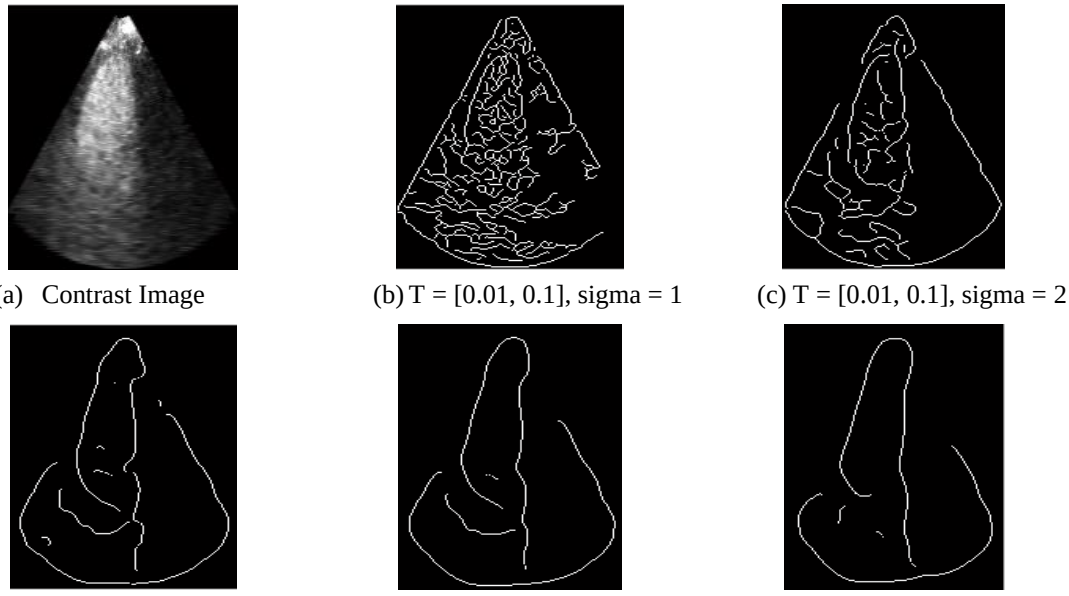

(a) Contrast Image (b) T = [0.01, 0.1], sigma = 1 (c) T = [0.01, 0.1], sigma = 2

(d) T = [0.01, 0.1], sigma = 4 (e) T = [0.01, 0.1], sigma = 5 (f) T = [0.01, 0.1], sigma = 7

Figure 2.15: Canny edge detection of left ventricle in contrast echocardiograph.

Therefore, applying conventional edge detection methods for LV feature extraction and segmentation do not offer effective results. The results of intensity-gradient based edge detectors (Sobel and Canny) demonstrate that it is hard to extract features from C3DE without pre-processing.

2.6 Preprocessing Method Application on C3DE Images

Section 2.2 has briefly explained the intensity transformation preprocessing methods for image subsequent analysis. The result of negative transformation on C3DE image from Figure 2.8 is not desirable because its appearance is not close to non-contrast image and by taking simple image negative (2.3)), image intensity variation would be same due to linear transformation nature, thus it is not possible to get its desired utilization.

Moreover, in this section logarithmic transformation (equation (2.4)) and power law transformation (equation (2.5)) are applied on C3DE images as a preprocessing step before feature extraction.

2.6.1 Log Transformation

A C3DE image is preprocessed with log transformation (constant value 2) and then LV cavity is extracted by Canny edge detector (see Figure 2.16). It has been observed that this transformation maps a narrow range of low intensity values of input into the wider range of output levels while keeping the brighter range approximately linear, so resultant image (Figure 2.16 (b)) has brighter myocardium border which reduces the low contrast change between LV brighter cavity and myocardium border. This result is also not useful in LV feature extraction (see Figure 2.16 (c))

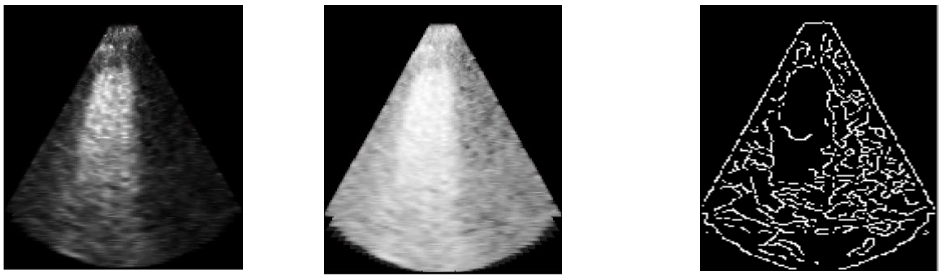

(a) Contrast Image (b) Log transformation, C = 2 (c) Canny, Th = [0.01, 0.1]

Figure 2.16: Log transformation of C3DE, (b) the results of log transformation with the constant value two and (c) the canny edge detection with the threshold value [0.01, 0.1].

2.6.2 Power Law Transformation

Another frequently used intensity level transformation is power law (equation (2.5)) transformation. In this transformation, using $\gamma<1$ brighten the darker part by expanding the narrow range of input values, whereas $\gamma>1$ compresses the narrow range and further expands the brighter range. This transformation is applied on C3DE image by changing γ values but still results are not satisfactory enough to lead the accurate cardiac LV volume assessment. However,

Figure 2.17 (b) shows the result of γ less than one and Figure 2.17 (e) shows the result of γ greater than one but both have not given suitable feature extraction results.

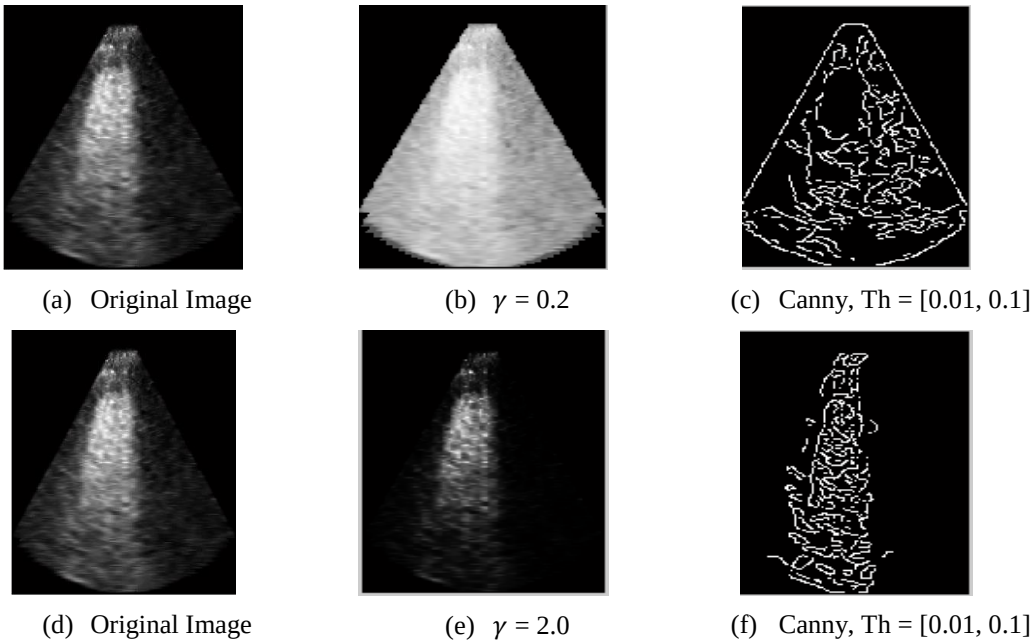

(a) Original Image (b) γ = 0.2 (c) Canny, Th = [0.01, 0.1]

(d) Original Image (e) γ = 2.0 (f) Canny, Th = [0.01, 0.1]

Figure 2.17 : Power law transformation of C3DE images.
Images (a) and (d) are original images, (b) are the results of power law transformation, where γ value is less than 1, (e) are the results of power law transformation, where γ value is greater than 1 and (c) and (f) results of canny feature extraction.

Moreover, the results of histogram based intensity transformation methods such as thresholding and contrast stretching are dependent on image properties. Hence one constant value for thresholding may not lead to accurate results. Our presented image inversion technique (will be discussed in next section) is also based on automatic threshold determination by C3DE image histogram analysis.

2.7 Summary

This chapter presented the background of cardiac imaging modalities. In this era, many imaging modalities are in use but echocardiography is the leading choice by the cardiologist because of its wide availability, cost effectiveness, no known harmful effects and portability. Real-time 3DE is a recent addition to the echocardiography imaging scene. The 3DE allows to capture and study the 3D morphology and dynamics of heart, at a low-cost and without associating any harmful effects. Despite the fact of being widely used in a large proportion of patients, 3DE may fail to produce diagnostically useful images. The image quality is known to be affected by ultrasound

physics and influenced by factors such as fat, rib spacing, ultrasound reflection angle, and lung disease. Therefore, C3DE has emerged as an alternative to improve image quality for such cases. Many cardiovascular diseases are associated with LV dysfunction, so LV segmentation is an active area in research.

This chapter also presented the issues related to the C3DE image appearance, which are responsible to make difficult and challenging image semi-automatic or automatic processing. Two main issues are: 1) Contrast inhomogeneity within LV cavity and 2) relatively low contrast between LV cavity and myocardium border which obstructs the LV feature extraction methods such as edge detection and region growing without introduction of preprocessing methods. In this regard, we have applied previous intensity level preprocessing techniques (i.e. log transformation and power law transformation) and extracted feature but results are unsatisfactory.

Therefore, C3DE LV segmentation is a challenging problem due to its difficult image quality and in this regard, we aim to develop image pre-processing technique for C3DE, which assists the subsequent image analysis such as LV segmentation. Our presented preprocessing technique is also based on intensity level transformation with the help of image histogram analysis

Chapter 3: Proposed Methodology

This chapter presents the methodology which is employed in this work. The proposed methodology is an adaptive pre-processing technique of inverse image construction in C3DE. The inverse of a C3DE image is constructed by finding a threshold value based on the image histogram properties.

3.1 Inverse Image Construction

In the C3DE images, LV cavity appears bright due to concentration of microbubbles contrast agent in blood pool, thus the visual appearance of C3DE is inverted compared to that of the 3DE (see Figure 1.2). We propose here to build an alternate inverse image representation, corresponding to a C3DE image, such that the blood pool noise is suppressed and the image contrast between blood pool and myocardium is enhanced. Accordingly, we attempt to build an image, from a C3DE image, which looks like a 3DE image. In this new representation, the blood pool appears dark and the myocardium appears bright which is inverse of the original image appearance. With this simple alternate representation trick, the segmentation methods proposed for 3DE images become applicable to C3DE inverse image.

Our method works by inverting very bright high-intensity pixels in LV cavity, while retaining the medium or low-intensity pixels unperturbed. For a given C3DE image I_c, the following intensity transformation is proposed to generate the inverse image I_i:

$$I_i(x,y,z) = \begin{cases} \dfrac{1}{I_c(x,y,z)}, & I_c(x,y,z) > T_h \\ I_c(x,y,z), & I_c(x,y,z) \leq T_h \end{cases} \tag{3.1}$$

where T_h is an intensity threshold specific to image properties. A threshold T_h is a specific intensity value, which differentiates the very bright high-intensity pixels (LV cavity) from medium-intensity (Myocardium) and low-intensity pixels. The result of above mentioned mapping is shown in Figure 3.1.

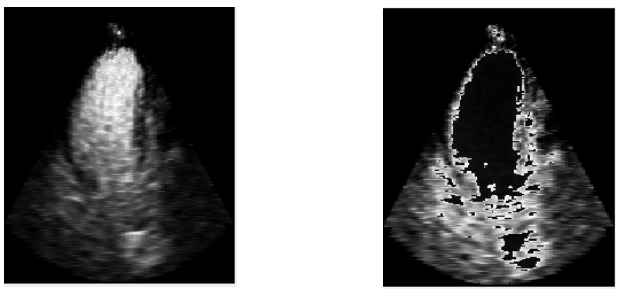

(a) C3DE image (b) Inverted C3DE image

Figure 3.1: C3DE inverse image construction.

We consider that the pixels with intensity value above T_h require to be inverted. The threshold T_h depends on the image intensity properties, therefore a universal constant value of threshold cannot be used for C3DE images. Thus, our primary contribution in image inverse construction is proposing an automatic method for threshold determination for a given C3DE image.

3.2 Threshold Estimation

Threshold estimation is a vital part of inverse image construction because it is tedious to find manual threshold for each new C3DE image. As described above, threshold T_h depends on image properties thus each C3DE image may have a different T_h value. For determination of T_h, our analysis is based on the C3DE dataset gray level histogram. Our proposed method is based on an initial training where threshold estimation is learned by the algorithm from the data analysis. Subsequently, the algorithm estimates the threshold automatically for a new C3DE image. The algorithmic steps of training process are described below:

a) Data analysis and training
    1. Histogram analysis
    2. Categorization of each C3DE image
    3. Manual threshold estimation of all C3DE image
    4. Frequency relationship estimation of each C3DE image
    5. Computing mean frequency relationship and mean peak frequency of the images within a category

b) Automatic threshold estimation
    1. Histogram analysis
    2. Categorization of a new C3DE image
    3. Find the displacement gap between current image peak frequency with a mean peak frequency of a category
    4. Finding the frequency relationship
    5. Finding the threshold value

Above steps are elaborated in the following section.

3.2.1 Data Analysis and Training

1. Gray level histogram shape analysis of a C3DE image by quantitatively calculating the bin percentage (bp) of first ten intensity bins:

$$\mathrm{bp}(r_{10}) = \frac{\sum_{k=1}^{10} h(r_k)}{\sum_{k=1}^{L-1} h(r_k)} * 100 \tag{3.2}$$

where r_k denotes intensity value, $h(r_k)$ denotes the frequency of intensity r_k, and $L-1$ is the largest intensity value. It is observed that histogram of C3DE dataset typically has one of the three different curve shapes while the $bp(r_{10})$ value indicates the shape of the curve. The three types of histograms are shown in Figure 3.2.

2. Based upon $bp(r_{10})$ value, the C3DE image f is categorized or placed into one of the three categories as below:

$$f \in \begin{cases} Cat1, & \mathrm{bp}(r_{10}) < bp1 \\ Cat2, & bp1 \leq \mathrm{bp}(r_{10}) < bp2 \\ Cat3, & \mathrm{bp}(r_{10}) \geq bp2 \end{cases} \tag{3.3}$$

where bp, $bp1$, and $bp2$ are constant values that differentiate amongst three categories of histogram shapes (as shown in Figure 3.2).

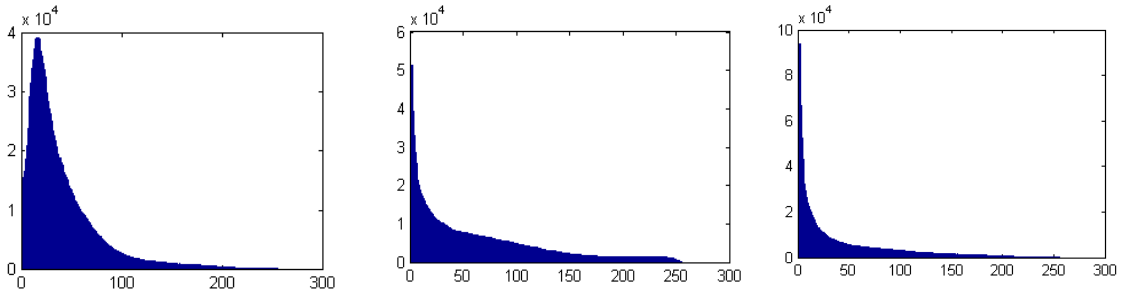

(a) Category 1 (b) Category 2 (c) Category 3

Figure 3.2 : Three types of C3DE image gray level histogram shapes,
x axis: gray intensity levels, y axis: Frequency of intensity levels

3. Find manual threshold (T_m) for each image, for the sake of training. The threshold represents an intensity value which separates the LV cavity and myocardium border and it has been obtained by visual analysis under expert guidance. This threshold is used to derive the automatic method for threshold estimation. Figure 3.3 (c) is showing an inverse image, which is constructed by a threshold value T_h (from the histogram Figure 3.4 (b)), which clearly separates the LV cavity and myocardium.

4. Find the relationship between frequency at manual threshold intensity value and the peak frequency of image f:

$$FR_{t/p}(r_t, f) = \frac{h(r_t)}{PF(f)} \tag{3.4}$$

$$\text{where, } PF(f) = max\left[h_f(r_k)\right] \tag{3.5}$$

$FR_{t/p}$ is the frequency relation between frequency at manual threshold $h(r_t)$ and peak frequency $PF(f)$ (see Figure 3.5). Within a category of C3DE images, the $FR_{t/p}$ values are found to be similar, thus by finding a $FR_{t/p}$ value of new image and $PF(f)$ from histogram, we believe that it can be helpful in estimating the threshold T_h automatically.

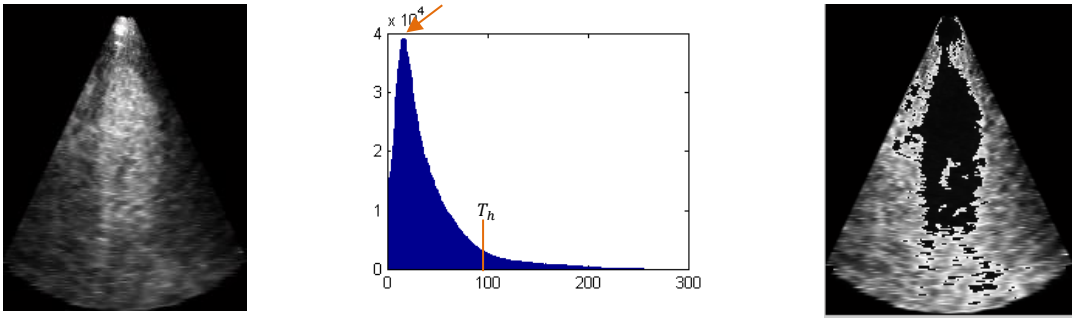

(a) C3DE image (b) C3DE image histogram (c) Image inversion by threshold

Figure 3.5: Inverted C3DE image using information from Histogram plot of C3DE image. (a) is an original image, (b) is image histogram, arrow is pointing the peak frequency $PF(f)$, and (c) is image inversion by using a threshold

5. Find the mean of $FR_{t/p}$ and peak frequency of all images within a category c:

$$\overline{FR}_{t/p}(c) = \frac{1}{N_c} * \sum_{i=1}^{N_c} FR_{t/p}(r_t, i) \tag{3.6}$$

$$\overline{PF}(c) = \frac{1}{N_c} * \sum_{i=1}^{N_c} PF(i) \tag{3.7}$$

where N_c is the number of images in category c, $\overline{FR}_{t/p}(c)$ is the mean of $FR_{t/p}$ for all images of category c, and $\overline{PF}(c)$ is the mean peak frequency for category c.

This now completes the description of steps required to train and obtains the values from data analysis which will be further used in ATE.

3.2.2 Automatic Threshold Estimation (ATE)

From the above analysis, it is noticed that frequency relationship $FR_{t/p}$ is similar within a category. Thus, any new C3DE image which falls in one of the above mentioned three categories would have its frequency relation $FR_{t/p}$ close to mean frequency relation $\overline{FR}_{t/p}(c)$. Therefore, we can find threshold T_h of a C3DE image by finding the $FR_{t/p}$ of that image. $FR_{t/p}$ of the C3DE image can be found by following steps:

1. Compute histogram of a new C3DE image f.
2. Image categorization based upon bin percentage $bp(r_{10})$.
3. Find the displacement gap $disp[PF(f)]$ of peak frequency (PF) of an image f with the mean peak frequency ($\overline{PF}$) of that category:

$$disp_{[PF(f),\ \overline{PF}(c)]} = \frac{PF(f) - \overline{PF}(c)}{\overline{PF}(c)} \tag{3.8}$$

4. Find the frequency relationship:

$$FR(f_x) = (1 - \alpha * disp) * \overline{FR}_{t/p}(c) \tag{3.9}$$

where α = 0.5 is found by empirical analysis.

5. Find the threshold frequency:

$$h(r_t) = PF(f) * FR(f_x) \tag{3.10}$$

Thus the intensity level with $h(r_t)$ frequency will be the image-specific threshold value T_h for a new C3DE image f.

3.3 Summary

This chapter presented the proposed methodology. It consisted of inverse image construction by a mapping in which pixel values greater than a specific threshold are inverted. For the threshold estimation, a relationship between threshold value and image peak frequency was found and a method was devised to estimate threshold automatically.

Chapter 4: Experiments and Results

This chapter discusses the validation of presented technique and the results obtained. As discussed in previous chapter, the proposed adaptive preprocessing technique comprises of an inverse C3DE image construction by automatic estimation of threshold value. Therefore, we have performed five different validation measures to assess the automatic threshold estimation. On the basis of automatic thresholding, inverse images are constructed and then validated by semi-automatic segmentation.

4.1 Implementation

The presented technique is implemented on C3DE images for image inversion.

4.1.1 Experimental Data

We obtained 16 C3DE scans, which were recorded at the Alberta University Hospital, Canada. The recordings were acquired with a volumetric matrix-array X5 probe using Philips iE33 ultrasound system. The image dimensions for each scan were either 160x144x208 or 192x176x208 depending on the settings of the ultrasound system.

4.1.2 Data analysis and training

All images are analyzed and trained according to the proposed steps i.e., as described in previous Chapter:

- Histogram analysis of each C3DE image by using equation (3.2), and categorizing according to equation (3.3).
- Manual threshold (T_m) value estimation of each C3DE image.
- Finding frequency relationship $FR_{t/p}$ value and peak frequency $PF(f)$ of each C3DE image by using equation (3.4) and ((3.5).
- Computing the mean frequency relationship and mean peak frequency for each image category.

All trained end diastolic (ED) data is presented in following tables: Table 4.1, Table 4.2 and Table 4.3 according to respective category. From the training, we noticed that commonly when peak frequency $PF(f)$ is greater than frequency relationship $FR_{t/p}$ is smaller and vice versa.

Table 4.1: Trained C3DE data of category 1				
#	bp(r_{10})	$FR_{t/p}$	$PF(f)$	T_m (intensity value)
1	9.5	0.17	31571	95
2	11.7	0.13	39236	80
$\overline{PF}(c_1)$ = 35403 $\overline{FR_{t/p}}(c_1)$ = 0.15				

Table 4.2: Trained C3DE data of category 2				
#	bp(r_{10})	$FR_{t/p}$	$PF(f)$	T_m (intensity value)
1	19.3	0.101	47324	90
2	19.5	0.094	51276	100
3	22.5	0.102	59101	75
4	22.7	0.083	71750	90
5	22.7	0.080	70822	90
6	22.9	0.088	67973	90
7	22.9	0.094	67576	90
$\overline{PF}(c_2)$ = 60827 $\overline{FR_{t/p}}(c_2)$ = 0.092				

Table 4.3: Trained C3DE data of category 3				
#	bp(r_{10})	$FR_{t/p}$	$PF(f)$	T_m (intensity value)
1	32.2	0.041	81706	80
2	33.2	0.039	93922	85
3	43.7	0.037	145298	65
4	44.5	0.037	148232	65
5	44.7	0.036	149624	65
6	44.9	0.037	149876	60
7	40.5	0.04	71677	75
$\overline{PF}(c_3)$ =120047 $\overline{FR_{t/p}}(c_3)$ = 0.038				

4.1.3 Automatic Threshold Estimation

Subsequent to training, we can estimate the threshold for a new C3DE test image by the following steps (section 3.2.2) i.e.

- Histogram computation of a new C3DE image and image categorization based upon bin percentage $bp(r_{10})$ by using equation (3.2) and (3.3) respectively.
- Finding the displacement gap (equation (3.8)) of peak frequency of current image with the mean peak frequency ($\overline{PF}$) of that category and then find the frequency relationship (3.9).
- And finally, find the threshold frequency by utilizing equation (3.10) and the threshold intensity level (T_h).

4.1.4 Inverse Image Construction

Inverse images are constructed by the proposed mapping in equation (3.1), while the threshold value T_h is automatically estimated. The inversion results are shown in Figure 4.1. These results assist the subsequent C3DE image analysis i.e. LV feature extraction and segmentation.

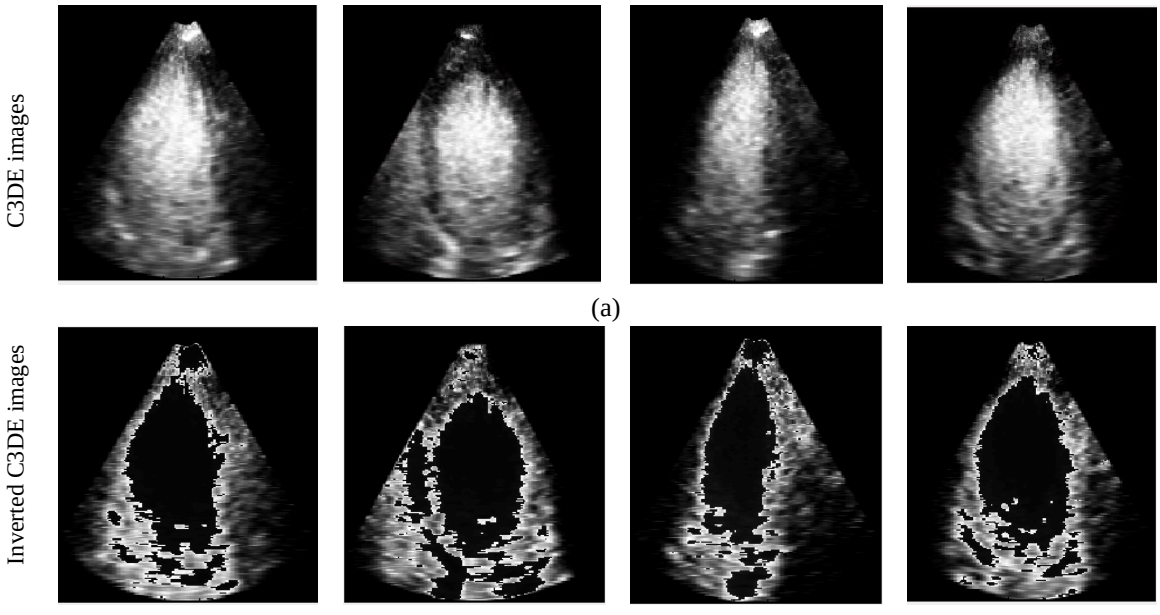

Figure 4.1: Results of C3DE image inversion by automatic threshold estimation

4.2 Validation Measures and Results

Automatic threshold estimation is validated through different measures for inverse image construction and then these inverse images are used in subsequent semi-automatic segmentation.

4.2.1 Validation of ATE

The proposed technique of automatic threshold estimation is initially trained on a collection of C3DE images, including end diastolic (ED) and end systolic (ES) frames. The performance of proposed method is validated by finding the mean of absolute difference error between the manual reference threshold (T_m) and automatic threshold ($T_{h)}$ of C3DE image:

$$E = |T_m - T_h| \tag{4.1}$$

$$\bar{E} = \frac{\sum_i E_i}{n} \tag{4.2}$$

where n is the number of images.

We present the validation conducted through various schemes, as below:

1. Training on ED images and validation on ED images - see Table 4.4 for results.
2. Training on ES images and validation on ES images - see Table 4.5 for results.
3. Training on ES images and validation on ED images - see Table 4.6 for results.
4. Training on ED images and validation on ES images - see Table 4.7 for results.
5. Leave one out validation of ES images and ED images collectively: the unbiased validation of proposed technique is carried out by leave-one out (LOO) cross validation. In LOO cross validation, for each of N experiments (N referring to total number of images), N-1 C3DE images were used in training and the trained algorithm was then tested on one excluded C3DE image. This process is performed N times to validate the whole dataset (see Table 4.8 for results).

Table 4.4: Results of validation, training on ED images and validation on ED images, Mean error ± standard deviation of automatic threshold estimation.

Category	# of C3DE images	$\bar{E}$	$\overline{PF}(c)$	$\overline{FR_{t/p}}(c)$
Category 1	2	2.5 ± 0.7	35403	0.152
Category 2	7	3.7 ± 2.6	60827	0.092
Category 3	7	5.7 ± 1.9	120047	0.038

Table 4.5: Results of validation, training on ES images and validation on ES images, Mean error ± standard deviation of automatic threshold estimation.

Category	# of C3DE images	$\bar{E}$	$\overline{PF}(c)$	$\overline{FR_{t/p}}(c)$
Category 1	2	0.5 ± 0.70	41520	0.119
Category 2	7	5.1 ± 2.9	63728	0.083
Category 3	7	5.4 ± 3.9	113305	0.034

Table 4.6: Results of validation, training on ES images and validation on ED images, Mean error ± standard deviation of automatic threshold estimation.

Category	# of C3DE images	$\bar{E}$	$\overline{PF}(c)$	$\overline{FR_{t/p}}(c)$
Category 1	2	5.5 ± 4.9	41520	0.119
Category 2	7	6.7 ± 3.1	63728	0.083
Category 3	7	9.8 ± 6.2	113305	0.034

Table 4.7: Results of validation, training on ED images and validation on ES images, Mean error ± standard deviation of automatic threshold estimation.

Category	# of C3DE images	$\bar{E}$	$\overline{PF}(c)$	$\overline{FR_{t/p}}(c)$
Category 1	2	4 ± 0	35403	0.152
Category 2	7	5.1 ± 4.6	60827	0.092
Category 3	7	7.6 ± 4.6	120047	0.038

Table 4.8: Results of LOO validation, Mean error ± standard deviation of automatic threshold estimation.		
Category	# of C3DE images	$\bar{E}$
Category 1	2	3.75 ± 2.9
Category 2	7	4.57 ± 3.5
Category 3	7	6.92 ± 5.6

4.2.2 Validation by Semi-Automatic Segmentation

As described previously, the inverse image construction brings the C3DE image appearance to match with the appearance of a 3DE image. This matching can be seen in Figure 4.2, in which an inverted C3DE image (Figure 4.2 (b)) and non-contrast 3DE image (Figure 4.2 (c)) both have dark LV cavity and brighter myocardium border contrary to C3DE image. The endocardial delineation is clearer with very little noise in the LV cavity blood pool and the image contrast has increased between the blood pool and the myocardium. Thus, the inverse image construction enables the application of a 3DE segmentation method on C3DE images.

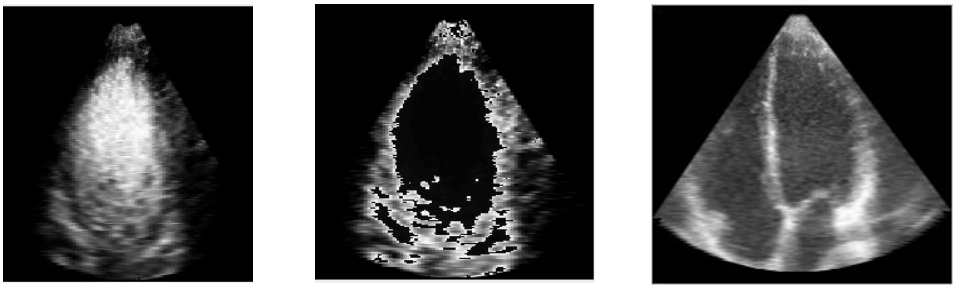

(a) C3DE image (b) C3DE image inversion (c) 3DE image

Figure 4.2: C3DE image inversion and non-contrast 3DE

We applied a traditional semi-automatic segmentation method, which is image-driven and derives its driving force from the image edges. The use of gradient based intensity edges for segmentation has become possible only as a result of inverse image construction. This segmentation method is based on 3D level set methods implementation of geodesic active contour [34] found in open-source software ITK-Snap [35]. We took total 32 2D slices, in which each 16 slices are from 2–chamber view and 4–chambered view. In order to test images from each category, we choose 8 slices from category (1),

12 slices from category (2), and 12 from category (3). The 2D slices from ED time point images were taken and the LV endocardial border was manually traced under the guidance of an expert cardiologist. The manually traced border was used as a ground truth to evaluate the traced LV endocardial border obtained from the proposed semi-automatic method. We used semi-automatic segmentation by stopping active deformable contour when it reaches the LV boundary. The segmentation results are shown in Figure 4.3 and Figure 4.4. As our scope was limited to image inversion, thus we decided to stick with two straight forward measures for quantitatively validating LV segmentation i.e. dice similarity index and mean contour distance.

1. Dice similarity index (DSI): DSI [36] is computed as a measure of area overlap between the reference contour (C_{ref}) and the automatic contour (C_{auto}), giving a measurement value between 0 (no overlap) and 1 (full overlap). DSI is measured as:

$$DSI = \frac{2(C_{ref} \cap C_{auto})}{C_{ref} + C_{auto}} \tag{4.3}$$

   where ∩ represent the intersection between the two contour. We have calculated the overlap of semi-automatic LV cavities with the ground truth segmented LV cavities and the DSI results are shown in Table 4.9.

2. Mean Contour Distance (MCD): The mean contour distance (d_{mean}) between the segmented contour line (C_{auto}) and reference contour line (C_{ref}) is defined as:

$$d_{mean} = \frac{1}{2}\left[\bar{d}\left(C_{ref}, C_{auto}\right) + \bar{d}\left(C_{auto}, C_{ref}\right)\right. \tag{4.4}$$

   where $\bar{d}\left(C_{ref}, C_{auto}\right)$ is the mean of distances between every contour pixel in reference contour and the closest contour pixel in auto contour. The MCD results are shown in Table 4.10.

Table 4.9: Results of Dice similarity index			
Category:	Category 1	Category 2	Category 3
Two chambered	0.92 ± 0.01	0.88 ± 0.02	0.85 ± 0.03
Four chambered	0.91 ± 0.01	0.89 ± 0.02	0.85 ± 0.03
Total mean	0.88 ± 0.03		

Table 4.10: Results of mean contour distance			
Category:	Category 1	Category 2	Category 3
Two chambered	1.44 ± 0.20 mm	2.15 ± 0.20 mm	2.65 ± 0.45 mm
Four chambered	2.50 ± 0.33 mm	2.62 ± 0.51 mm	3.29 ± 0.66 mm
Total mean	2.49 ± 0.59 mm		

4.3 Discussion

This section discusses the results.

4.3.1 Automatic Threshold Estimation (ATE)

The presented algorithm, trained on 32 C3DE images (16 ED and ES images each), was used to estimate the threshold automatically. The performance of ATE of threshold T_h through five validation schemes is presented in Table 4.4 to Table 4.8 respectively, which demonstrates the close match with manual threshold T_m with reasonable mean error.

In our analysis, we observed that the variation in threshold value by up to 10 points (intensity level) is tolerable. In automating threshold estimation, first two validation schemes are considered to be biased because same images are used in training and validation (Table 4.4 and Table 4.5). From their result, we can deduce that the maximum error of 5.7 ± 1.9 for ED time images and 5.4 ± 3.9 on ES images is quite acceptable. Next three validation schemes are completely unbiased since the algorithm is trained and validated on different images. However unbiased training of ES images and then validation on ED images (see Table 4.6) yields the mean error of 9.8 ± 6.2 of category 3, but we consider it acceptable as it is under the tolerable value range. Moreover, the results of fourth (ED training, ES validating) and fifth (LOO) validation are given in Table 4.7 and Table 4.8 respectively, which have maximum mean errors of 7.6 ± 4.6 and 6.92 ± 5.6 respectively, which is well within the tolerable limit of threshold.

Another point noticed from the analysis is that maximum threshold mean error belongs to third category in every validation schemes set. The possible reason for maximum error is the diverse properties (i.e. curve, peak frequency etc.) of C3DE images that fall in this category.

4.3.2 Semi-Automatic Segmentation

The qualitative results of image inversion and subsequent LV segmentation are presented in Figure 4.3 and Figure 4.4. The native C3DE image is shown in Figure 4.3 (a) and Figure 4.4 (a). The gradient information in Figure 4.3 (b) and Figure 4.4 (b) clearly shows that it is hard to extract LV cavity from C3DE image without pre-processing. The inverted image constructed by the proposed method from C3DE image is shown in Figure 4.3 (c) and Figure 4.4 (c).

We can observe (see Figure 4.3 (c) and Figure 4.4 (c)) that the inverse image has appearance very similar to the 3DE image. This new inverse appearance makes it possible to employ an image-driven LV segmentation method. According to gradient information of inverse image (Figure 4.3 (d) and Figure 4.4 (d)), the LV cavity is clearer, which can be relatively easily segmented. The results of segmentation are shown in Figure 4.3 (e) and Figure 4.4 (e), which clearly show reasonable segmentation accuracy. Figure 4.3 (f) and Figure 4.4 (f) show the visual overlay comparison of reference contour (i.e. ground truth), obtained by manual delineation, with the contour obtained through the semi-automatic image-driven method. We can observe a close match between the reference and semi-automatic contours. It clearly shows that the LV segmentation becomes possible by image inversion method.

Moreover, the quantitative evaluation using dice similarity index (DSI) and mean contour distance (MCD) of image inversion and subsequent LV segmentation are presented in Table 4.9 and Table 4.10, respectively. The evaluation was conducted separately for apical 4-chamber, apical 2-chamber slices since the reference contours were available for these slices.

Table 4.9 shows the DSI values for segmentation performance at ED time points in the cardiac cycle. It is observed that the DSI mean value of 2 - chamber view and 4 - chamber view illustrate a better overlap of the LV reference contour and automatic contour cavity. From Table 4.9, DSI value of 2-chamber and 4 - chamber view against

each category shows that overlap is quite satisfactory. Table 4.10: Results of mean contour distance shows the MCD values between the reference and semi-automatic contours at both the 2 - chamber and 4 – chamber views in ED. The average MCD error across all 3 categories is 2.49 ± 0.59 mm which is not too high and fairly acceptable.

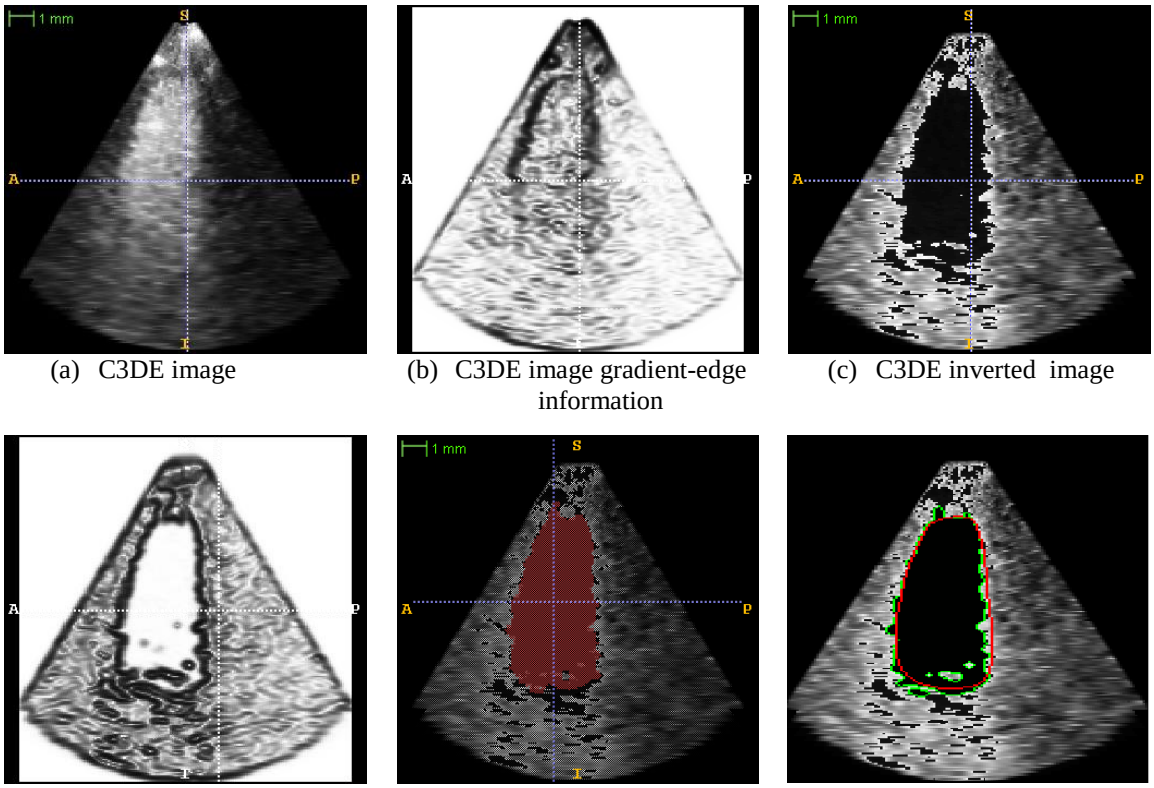

(a) C3DE image (b) C3DE image gradient-edge information (c) C3DE inverted image

(d) C3DE inverted image gradient-edge information (e) C3DE LV segmentation (f) Segmentation overlay result

Figure 4.3: C3DE segmentation process and the obtained result. (f) is an overlay of reference LV boundary (in red) and segmented LV boundary (in green).

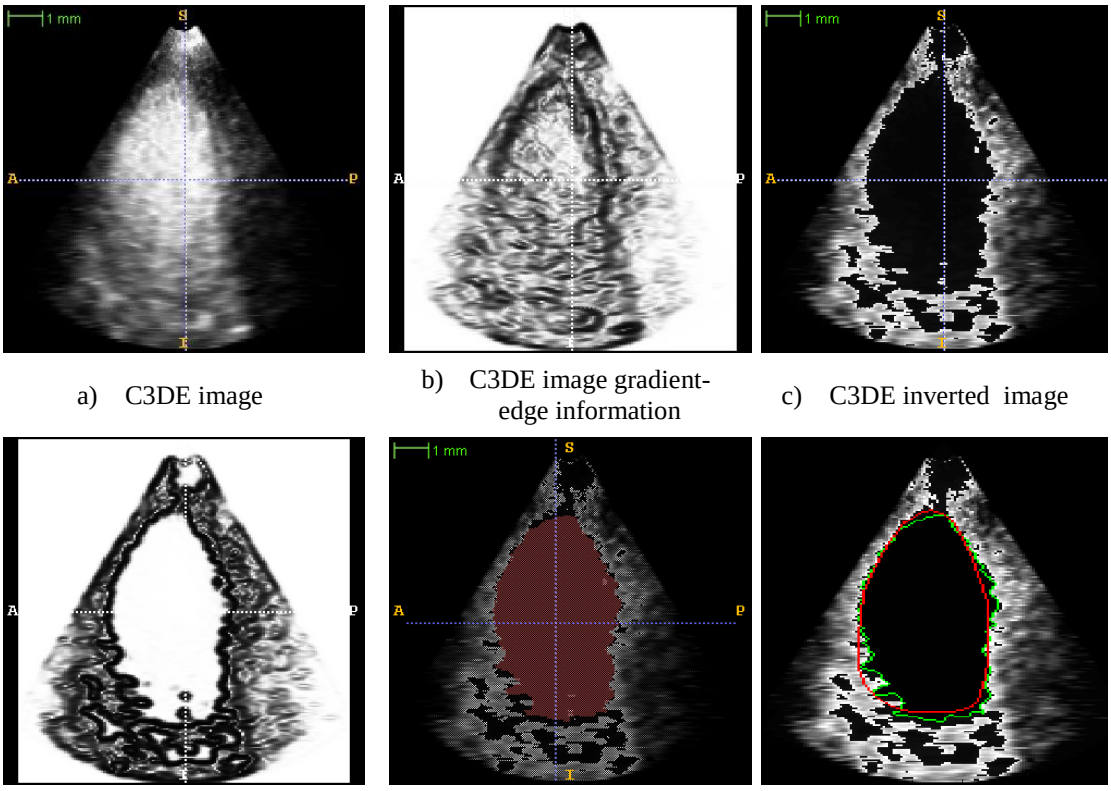

a) C3DE image

b) C3DE image gradient-edge information

c) C3DE inverted image

d) C3DE inverted image gradient-edge information

e) C3DE LV segmentation

f) Segmentation overlay result

Figure 4.4: C3DE segmentation process and the obtained result. (f) is an overlay of reference LV boundary (in red) and segmented LV boundary (in green).

For comparison of segmentation results, as mentioned earlier (section 2.3) only Ma et al. [5] worked on LV segmentation from C3DE, but they have used different validation schemes than DSI and MCD and due to our limited scope towards segmentation, we chose not to utilize their validation schemes. Another reason of not comparing is that they used C3DE scans which were obtained from a fast rotating ultrasound transducer (FRU), their C3DE image properties are different and slightly better than of matrix array transducers C3DE images, thus their comparison is not so worthy. However, these DSI and MCD errors are comparable to error reported earlier in literature for real-time 3DE segmentation and is within the inter-rater and intra-rater variability. Rajpoot and Noble [15] reported real-time 3DE LV segmentation DSI and MCD 0.88 ± 0.04 and 1.93 ± 0.62 mm, respectively. We note that image quality of C3DE image is more challenging and, therefore quantitative validation further verifies our claim regarding the similarity between manual and semi-automatic LV delineation.

4.4 Summary

This chapter presented the validation and discussed the results. Since our main aim was to develop an adaptive preprocessing technique of image inversion, therefore we validated it with different validation schemes.

We validated ATE with two biased and three unbiased validation schemes and achieved favorable results. The inverse image was utilized for LV segmentation of C3DE images and acquired satisfactory results. The results demonstrate that the inverse appearance of contrast image enables and simplifies the subsequent LV segmentation process.

Chapter 5: Conclusion and Future Work

This chapter concludes the thesis and suggests future work directions.

5.1 Conclusion

Though 3DE is the foremost choice by cardiologist to assess cardiac structure and function, but at times it fails to produce diagnostically useful images due to obesity, lung breathing, skin and tissues reduce the signal to noise ratio. Therefore, C3DE is used as alternative to overcome these limitations and cardiologists prefer contrast echocardiography in those cases where non contrast echocardiography results are unsatisfactory.

We have explored that C3DE enhances the visual quality of ultrasound images in comparison with 3DE. Though the image quality in C3DE is perceived to be improved for visual analysis, but it actually deteriorates for the purpose of automatic or semi-automatic analysis due to high speckle noise and intensity inhomogeneity. Two main issues are identified in this work: 1) Contrast inhomogeneity within LV cavity, and 2) relatively low contrast between LV cavity and myocardium border. These issues obstruct the LV feature extraction methods. Moreover, the LV endocardial segmentation from C3DE images remains a challenging problem with the little work conducted in this area.

To deal with this challenge, we presented a simple adaptive preprocessing method to invert the appearance of C3DE image. This inverted appearance yields low noise appearance, strong LV endocardium boundary and facilitates feature extraction for segmentation. As image inversion mapping is carried out by using intensity threshold value hence our major contribution in this work is presenting an automatic threshold estimation method by histogram analysis.

This technique is validated through qualitative and quantitative means and favorable results were found.

This research work is the first attempt of its kind towards preprocessing technique and automatic/semi-automatic LV segmentation from C3DE images and a part of thesis work has been accepted in the 12th International Conference on Frontier of Information Technology (Islamabad, Pakistan), entitled “An Adaptive Inverse Image Construction Method for Contrast 3D Echocardiography”.

5.2 Future Work

As described above, this work is first attempt towards C3DE image preprocessing technique; therefore many future directions can be explored.

5.2.1 Validation on Larger Dataset

In this work, the data analysis/training and validation has been performed on limited set of C3DE image, hence we cannot reliably predict the accuracy of results if any new C3DE image has a different bin percentage ($bp(r_{10})$) value from previously trained set values. Therefore, this work can be extended in future by applying and validating the proposed inversion technique on a larger size dataset.

5.2.2 C3DE Image Homogenization

C3DE image inhomogeneity is an important issue, therefore an image enhancement technique can be developed for C3DE images homogenization. In image inversion, the homogenization might help in smoothness of endocardial border. Figure 5.1 is showing the inhomogeneous LV region of a C3DE image. For image homogenization, the concern is to homogenize the local intensity values of LV cavity. Therefore, this method can be based on piecewise intensity thresholding.

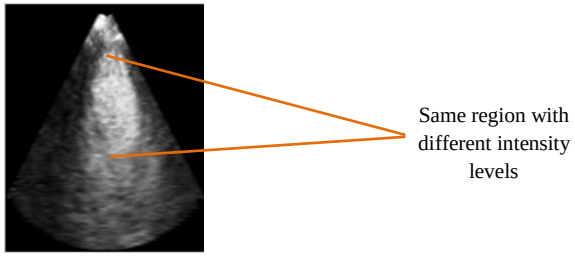

Figure 5.1: 2D slice of contrast 3D echocardiography.

The homogenization can be achieved by following steps:

1. Two thresholds value say high_thresh and low_thresh would be calculated from image intensity contents
2. Applying mask on the basis of calculated thresholds on the contrast image
3. Upscaling the selected pixels value by multiplying with a scaling factor

The above steps can be explored and might be helpful in development of image homogenization.

5.2.3 3DE Image Segmentation Methods and Commercial Tools

For C3DE images, there is no availability of commercial segmentation tools and 3DE tools (QLAB and TomTec) do not offer support to C3DE image segmentation. Since we have explained that a C3DE inverse image has appearance like non contrast 3DE image, therefore it can be explored that inverse image could be segmented on those commercial tools and by 3DE

segmentation methods. A detailed study on this topic could shed light upon the application of 3DE methods and commercial tools on the inverse images.

5.2.4 Comparison of C3DE Images with Non-Contrast 3DE

Cardiologists prefer contrast images over non contrast, in particular when corresponding non-contrast image quality is poor and hinder cardiac assessment. Therefore this can be a research direction that whether comparison of C3DE inverted image (appearance like non-contrast image) and 3DE of same patient could assist the cardiologist for better cardiac assessment.

References

[1] M. Nichols, N. Townsend, R. Luengo-Fernandez, J.Leal, A. Gray, P. Scarborough, and M. Rayner, "European Cardiovascular Disease Statistics 2012," *European Heart Network, Brussels, European Society of Cardiology, Sophia Antipolis,* 2012.

[2] J. Hung, R. Lang, F. Flachskampf, S. K. Shernan, M. L. McCulloch, D. B. Adams, J. Thomas, M.Vannan, and T. Ryan, "3D echocardiography: a review of the current status and future directions," *Journal of the American Society of Echocardiography,* p. 20, 2007.

[3] Jenkins, K. Bricknell, L. Hanekom, and T. Marwick, "Reproducibility and Accuracy of Echocardiographic Measurements of Left Ventricular Parameters Using Real-Time Three-Dimensional Echocardiography," *Journal of the American College of Cardiology,* vol. 44, 2004.

[4] R. Senior, H. Becher, M. Monaghan, L. Agati, J. Zamorano, J. L. Vanoverschelde, and P. Nihoyannopoulos, "Contrast echocardiography: Evidence-based recommendations by European Association of Echocardiography," *European Journal of Echocardiography* 2009.

[5] K. Rajpoot, J. A. Noble, and V. Grau, "Image-Driven Cardiac Left Ventricle Segmentation for the Evaluation of Multiview Fused Real-Time 3-Dimensional Echocardiography Images," *Medical Image Computing and Computer Assisted Intervention,* p. 8, 2009.

[6] H. Becher and P. N. Burns, "Handbook of contrast echocardiography: Left ventricular function and myocardial perfusion," *Springer Verlag,* 2000.

[7] M. Ma, M. v. Stralen, Johan, Reiber, J. G, Bosch, and Boudewijn, "Left Ventricle Segmentation from Contrast Enhanced Fast Rotating Ultrasound Images Using Three Dimensional Active Shape Models," *Functional Imaging and Modeling of the Heart,* 2009.

[8] M. Garbi, "The general principles of echocardiography " in *The EAE Textbook of Echocardiography*, ed: Oxford University Press, 2011.

[9] R. Gowda, I. Khan, B. Vasavada, T. Sacchi, and R. Patel, "History of Evolution of Echocardiography," *International Journal of Cardiology,* p. 6, 2004.

[10] A. M. Abdulla. Available: http://www.heartsite.com/html/tee.html

[11] R. C. Houck, J. E. Cooke, and E. A. Gill, "Live 3D Echocardiography: A Replacement for Traditional 2D Echocardiography?," *American Journal of Roentgenology*, vol. 187, pp. 1092-1106, 2006/10/01 2006.

[12] A. Fenster, D. Downey, and N. Cardinal, "Three-Dimensional Ultrasound Imaging," *Physics in Medicine and Biology*, vol. 46, p. 32, 2001.

[13] T. S, N. RF, and S. KB, "Use of contrast for image enhancement during stress echocardiography is cost-effective and reduces additional diagnostic testing," *American Journal of Cardiology*, 2001.

[14] G. R and S. PM., "Echocardiography of the aortic root," *Investigating Radiology* vol. 3, p. 10, 1968.

[15] K. M. Rajpoot, "Multi-view 3D Echocardiographic Image Analysis," Doctor of Philosophy, Institute of Biomedical Engineering, Department of Engineering Science, University of Oxford, 2009.

[16] C. Marcu, A. Beek, and A. V. Rossam, "Clinical Applications of Cardiovascular Magnetic Resonance Imaging," *Canadian Medical Association Journal*, 2006.

[17] K. Nayak and B. Hu, "The Future of Real-time Cardiac Magnetic Resonance Imaging," *Current Cardiology Reports*, vol. 7, p. 6, 2005.

[18] R. C. Gonzalez and R. E. Woods, *Digital Image Processing*: Prentice Hall, 2007.

[19] R. Maini and H. Aggarwal, "A Comprehensive Review of Image Enhancement Techniques " *Journal Of Computing*, vol. 2, p. 6, 2010.

[20] Zwim and Akselrod, "A Histogram-Based Technique for Echocardiographic Image Enhancement," *IEEE Computers in Cardiology* 2004.

[21] P. C. Tay, Christopher, Garson, S. T, Acton, and J. A. Hossack, "Ultrasound Despeckling for Contrast Enhancement," *IEEE Transactions On Image Processing*, vol. 19, p. 14, july 2010.

[22] H. Cheng and W. Tang, "A Robust Denoising for Medical Ultrasound Image based on SVR Estimation in Wavelet Domain," *Bioinformatics and Biomedical Engineering*, p. 4, 2008.

[23] D.-C. Chang and W.-R. Wu, "Image Contrast Enhancement Based on a Histogram Transformation of Local Standard Deviation," *IEEE Transactions On Medical Imaging,* vol. 17, p. 14, August 1998.

[24] Trussell and Hunt, "Nonstationary assumption for Gaussian models of images," *IEEE Transactions on Systems, Man, and Cybernetics,* vol. SMC-6, p. 6, 1978.

[25] J. Modersitzki and S. Wirtz, "Combining Homogenization and Registration," *Biomedical Image Registration: Third International Workshop,* p. 7, 2006.

[26] N. F. Voelkel, R. A. Quaife, L. A. Leinwand, R. J. Barst, M. D. McGoon, D. R. Meldrum, J. Dupuis, C. S. Long, L. J. Rubin, F. W. Smart, Y. J. Suzuki, M. Gladwin, E. M. Denholm, and D. B. Gail, "Right Ventricular Function and Failure; Report of a National Heart, Lung, and Blood Institute Working Group on Cellular and Molecular Mechanisms of Right Heart Failure," *American Heart Association, Inc.,* p. 9, 2006.

[27] J. A. Noble and D. Boukerroui, "Ultrasound Image Segmentation: A Survey," *IEEE Transactions On Medical Imaging,* vol. 25, p. 24, August, 2006.

[28] C. Domain. (2014). *Aortic Valve Disease*. Available: http://www.virginiaheart.com/

[29] M. Mignotte and J. Meunier, "A multiscale optimization approach forthe dynamic contour-based boundary detection issue," *Computer Medical Imaging Graph,* vol. 3, p. 10, 2001.

[30] Z. V, W. V, C.-P. CR, Q. JX, S. JM, and S. R., "Registration-assisted segmentation of real-time 3-D echocardiographic data using deformable models.," *IEEE Transaction Medical Imagaging,* vol. 24, p. 10, 2005.

[31] X. Chenyang and J. L. Prince, "Snakes, shapes, and gradient vector flow," *Image Processing, IEEE Transactions on Image Processing,* vol. 7, pp. 359-369, 1998.

[32] E. D. Angelini, A. F. Laine, S. Takuma, J. W. Holmes, and S. Homma, "LV volume quantification via spatiotemporal analysis of real-time 3-D echocardiography," *IEEE Transaction Medical Imagaging* vol. 20, p. 12.

[33] S. Deopujari and Y. Dubeys, "Segmentation of Left Ventricle of Echocardiographic image using Active contouring," *International Conference on Computational Intelligence and Communication System,* 2011.

[34] V. Caselles, R. Kimmel, and G. Sapiro, " Geodesic Active Contours," *International Journal of Computer Vision,* vol. 22, p. 18, 1997.

[35] P. A. Yushkevich, J. Piven, H. C. Hazlett, R. G. Smith, S. Ho, J. C. Gee, and G. Gerig, "User-guided 3D Active Contour Segmentation of Anatomical Structures: Significantly Improved Efficiency and Reliability," *NeuroImage,* vol. 31, p. 12, 2006.

[36] L. R. Dice, "Measures of the Amount of Ecologic Association Between Species," *Ecology,* vol. 26, p. 6, July 1945.